

A new proposal to Jefferson Lab PAC-28
The Δd Experiment:
Constraining d -Quark Polarization through Semi-Inclusive
Spin Asymmetry Measurements on a Polarized ${}^3\text{He}$ Target

(A Jefferson Lab Hall A Collaboration Experiment)

R. Gilman, C. Glashausser, X. Jiang (Spokesperson)^a, E. Kuchina, G. Kumbartzki,
R. Ransome
Rutgers University, Piscataway, New Jersey.

P. Markowitz
Florida International University, Miami, Florida.

P. Bosted, J.-P. Chen, E. Chudakov, R. Feuerbach, J. Gomez, O. Hansen,
D.W. Higinbotham, C. W. de Jager, M. Jones, J. .J. LeRose, R. Michaels, S. Nanda,
B. Reitz, A. Saha
Thomas Jefferson National Accelerator Facility, Newport News, Virginia.

L. Zhu
University of Illinois, Urbana-Champaign, Illinois.

J. R. Calarco
University of New Hampshire, Durham, New Hampshire.

D. Armstrong, T. Averett, T. Holmstrom, V. Sulkosky
College of William and Mary, Williamsburg, Virginia.

D. Day, R. Lindgren, N. Liyanage, V. Nelyubin, B. Norum, K. Slifer, K. Wang
University of Virginia, Charlottesville, Virginia.

Y. Jiang, H. Lu, Y. Ye
University of Science and Technology of China, Hefei, P.R.China.

S. Zhou
China Institute of Atomic Energy, Beijing, P.R.China.

E. Cisbani, F. Cusanno, S. Frullani, F. Garibaldi, S. Marrone, G. Urciuoli, M. Iodice,
R. De Leo, L .La Gamba
INFN Roma-I, INFN Roma-III, INFN Bari and University of Bari, Italy.

S. Širca

^aemail: jiang@jlab.org

University of Ljubljana, Slovenia.

Seonho Choi
Seoul National University, Seoul, Korea

J.R.M. Annand, G. Rosner
University of Glasgow, Glasgow, Scotland, United Kingdom.

Abstract: We propose to measure the beam-target double-spin asymmetries in semi-inclusive deep-inelastic $\vec{n}(\vec{e}, e' \pi^+) X$ and $\vec{n}(\vec{e}, e' \pi^-) X$ reactions (kaons as by-products) on a longitudinally polarized high luminosity ${}^3\text{He}$ target. Since the neutron asymmetries are most sensitive to d -quark polarization, this experiment will dramatically improve our knowledge of $\Delta d(x)$. In addition, since the hadron phase spaces and detection efficiencies will be well-controlled in this experiment, the combined asymmetry $A_{1\text{He}}^{\pi^+ - \pi^-}$, in which the gluon contributions cancel out exactly to all orders of QCD, will be determined with high precision. The newly constructed BigBite spectrometer, in the same detector configuration as in the Hall A “ G_{En} ”, will be used to detect the scattered electrons at 30° . The left-HRS spectrometer, with its septum magnet at 6° , will be used to detect the leading hadrons in coincidence ($p_h = 2.4 \text{ GeV}/c$, $z \approx 0.5$). The high statistics data from this experiment will also be used as inputs to a global NLO QCD analysis to put strong constraints on quark helicity distributions, and indirectly constrains gluon polarization to the level comparable to that from RHIC-spin. When combined with the proton data of the Hall C semi-SANE experiment, this experiment will definitely provide us with the first opportunity to discover the possible polarized sea asymmetry $\Delta \bar{u} - \Delta \bar{d}$. All experimental apparatus exist in Hall A and no special requirement is needed for the BigBite detectors beyond its standard configuration in the “ G_{En} ” experiment. A total of 24 days of 6 GeV beam in Hall A is requested.

Contents

1	Introduction	5
2	Physics Motivation	7
2.1	Beam-target double-spin asymmetries at leading order	7
2.2	HERMES results from leading order purity method	8
2.3	Neutron asymmetries are sensitive to Δd	9
2.4	SIDIS Cross sections at the next-to-leading order	10
2.5	NLO global QCD analysis of DIS and SIDIS data	11
2.6	Methods of spin-flavor decomposition	12
	LO Christova-Leader method to obtain $\Delta u_v(x)$, $\Delta d_v(x)$ and $\Delta \bar{u}(x) - \Delta \bar{d}(x)$	12
	NLO Christova-Leader method	13
	Cross check Δq_v with the upgraded RHIC	14
	The leading-order “fixed- z purity” method	14
2.7	$\Delta \bar{u} - \Delta \bar{d}$: the flavor asymmetry in the polarized sea	14
2.8	The target single-spin asymmetry A_{UL}	15
2.9	Recent JLab data suggests leading order naive $x - z$ factorization . .	17
3	The Proposed Measurement	18
3.1	Overview	18
3.2	Kinematics and phase space	19
3.3	The experimental observables	20
3.4	The electron arm: BigBite	22
	Single particle background and track reconstruction in BigBite . .	25
3.5	The hadron arm: HRS+septum	25
3.6	Trigger and offline event selection	26
3.7	The polarized ${}^3\text{He}$ target	27
	Effects of BigBite and septum magnetic field	27
4	Event Rate Estimate and Statistical Uncertainties	28
4.1	Cross section and rate estimate	28
4.2	Statistical uncertainties on raw asymmetries	29
4.3	Statistical uncertainties on physics asymmetries and Δd_v	29
4.4	Systematic uncertainties	30
	Systematic uncertainty of $A_{{}^1\text{He}}^h$ and $A_{{}^1n}^h$	30
	Effective nucleon polarization in ${}^3\text{He}$	31
	π - N final state interaction	32
	Target fragmentation and vector meson production	32
	Corrections from non-vanishing A_\perp^n	32
	Systematic uncertainty of Δq , $\Delta \bar{u} - \Delta \bar{d}$	33

5 Beam time request, hardware costs and installation time needed	34
5.1 Beam time request	34
5.2 Hardware costs and installation time needed	34
6 The Expected Results	35
6.1 Double spin asymmetries A_{1He}^h and A_{1n}^h	35
6.2 Flavor decomposition of quark polarization and the impacts to NLO global fits	35
$\Delta d_v(x)$ from the leading-order Christova-Leader method	35
$\Delta \bar{u}(x) - \Delta \bar{d}(x)$ from the leading-order Christova-Leader method	35
Leading-order quark polarization of all flavor	35
Impact to NLO QCD global fit: sea and gluon polarization moments	39
7 Relation with other experiments	40
8 Collaboration and responsibility	42
9 Summary	42
A HERMES purity method and results	44
B Details of flavor decomposition	47
B.1 Spin-dependent and spin-independent cross sections	47
B.2 The asymmetries expressed in “fixed- z purity”	48
C NLO global fit to DIS and SIDIS Data	48
D Comparison of statistical uncertainties with semi-SANE	48

1 Introduction

The last decade has seen remarkable progress in the knowledge of the polarized parton distribution functions (pPDF) $\Delta q_f(x)$. The most precise and clearly interpreted data are from inclusive deep-inelastic lepton scattering (DIS) experiments at CERN and SLAC. However, the information available from inclusive DIS process has inherent limitations. As the cross sections are only sensitive to e_q^2 , the quark charge square, an inclusive experiment probes quarks and anti-quarks on an equal footing, and it is only possible to determine combinations of $\Delta q + \Delta \bar{q}$, but never Δq_v and $\Delta \bar{q}$ separately. Therefore it is not sensitive to the symmetry breaking in the sea sector. Only one particular flavor non-singlet can be directly inferred through DIS measurements, i.e. $\Delta q_3(x, Q^2) = \Delta u + \Delta \bar{u} - \Delta d - \Delta \bar{d}$. The additional assumption of $SU(3)_f$ flavor symmetry allows the hyperon beta decay data to constrain the first moments of Δq . The well-cited result of this approach is that quark helicities seem to make a small net contribution to the nucleon spin, and the strange sea appears to be negatively polarized.

The sensitivity to each individual quark flavor is realized in semi-inclusive deep inelastic scattering (SIDIS) in which one of the leading hadrons is also detected. Since the leading hadrons from the current fragmentation carry information about the struck quark's flavor, detection of the leading hadron effectively “tags” the quark flavor. Therefore, SIDIS offers an unique opportunity for determining the spin, flavor, and sea structure of the nucleon¹, thereby significantly enriching our understanding of QCD and the nucleon structure. High precision polarized SIDIS data on the proton and the neutron allows a flavor decomposition of nucleon spin structure, which could lead to the discovery of a possible flavor-asymmetry in the polarized sea. Recently, the HERMES collaboration published the results of a leading order spin flavor decomposition from polarized proton and deuteron data, and for the first time extracted the sea quark polarizations^{2,3}. Unlike the predictions of several theoretical models, HERMES found that within the available statistics $\Delta \bar{u} - \Delta \bar{d}$ is consistent with an unbroken $SU(2)_f$ symmetry.

The HERMES data has demonstrated that, within the experimental precision, the semi-inclusive double-spin asymmetries A_{1N}^h at $\langle Q^2 \rangle = 2.5 \text{ GeV}^2$ agree reasonably well with the SMC data⁴ which was obtained at $\langle Q^2 \rangle = 10 \text{ GeV}^2$. Recent Jefferson Lab Hall B results⁵ of $A_{1p}^{\pi^+}$ asymmetry, which is at $\langle Q^2 \rangle = 1.8 \text{ GeV}^2$, are also shown to be consistent with HERMES and MC data. This non-trivial agreement indicates that the expected violation of leading order x - z factorization is not large around Q^2 of 2.0 GeV^2 , and the semi-inclusive asymmetry has a rather weak Q^2 dependence. Recent JLab E08-108 data⁶, on unpolarized SIDIS cross section ratios of proton and deuteron, also indicates that the leading order naive x - z factorization is rather close to the reality. This apparent “precocious scaling” suggests that at modest Q^2 , information on the quark distributions is reasonably well-preserved in semi-inclusive reactions. Recently, Ji, Ma and Yuan explicitly proved⁷ that QCD factorization is valid for SIDIS with hadrons emitted in the current fragmentation region with

low transverse momentum $p_{\perp h} \ll Q$. QCD factorization of spin-dependent cross sections in SIDIS and Drell-Yan has also been proved for the low $p_{\perp h}$ case⁸. A schematic strategy of leading order x - z factorization test was suggested⁹ which requires prior knowledge of neither fragmentation functions nor parton distributions. The experimental challenge in this strategy is to measure the combined double-spin asymmetry $A_{1N}^{\pi^+ + \pi^-}$. If leading order factorization holds perfectly, $A_{1N}^{\pi^+ + \pi^-}$ will turn out to be identical to the inclusive A_{1N} asymmetry due to the exact cancellation of the fragmentation functions. Their difference, $A_{1N}^{\pi^+ + \pi^-} - A_{1N}$, gives a clear indication on the size of the next-to-leading-order terms which violate the naive leading order x - z factorization. In practice, the combined asymmetry $A_{1N}^{\pi^+ + \pi^-}$ poses more experimental challenges, since knowledge of phase spaces and detection efficiencies are required.

Similar to the approved Hall C semi-SANE experiment¹⁰ (E04-113), this experiment is specifically designed to have well controlled phase spaces and hadron detection efficiencies such that the combined asymmetries $A_{1He}^{\pi^+ \pm \pi^-}$, in addition to the individual asymmetries A_{1He}^h , can be determined with high precision to give a better lever-arm in the flavor decomposition. At Q^2 of $1.21 \sim 3.14$ GeV², a leading order spin-flavor decomposition of the nucleon spin structure will be performed in the region of $x = 0.12 \sim 0.41$. The much improved statistics on the ${}^3\text{He}$ target, when combined with the expected Hall C semi-SANE proton data, will provide us with the first opportunity to discover the possible polarized sea asymmetry. It was pointed out by Christova and Leader⁹ that if the combined asymmetries $A_{1N}^{\pi^+ - \pi^-}$ are measured with high enough precision, quark polarization Δu_v , Δd_v and $\Delta \bar{u} - \Delta \bar{d}$ can be extracted at leading order independent of the knowledge of fragmentation functions. Even at the next-to-leading order, information on the valence quark polarizations is well-preserved in the combined asymmetries $A_{1N}^{\pi^+ - \pi^-}$.

At the next-to-leading order, following the well established formalism¹¹, tools of NLO QCD global fits, which include data sets from both inclusive and semi-inclusive reactions, have become available recently¹². The high statistics data from this experiment, adding neutron asymmetries to the world data, will serve as stringent constraints on pPDFs through NLO global fits. Indirectly, the constraint on Δg coming from the addition of data of this experiment is as stringent as the projected $A_{LL}^{\pi^0}$ data from PHENIX-2007 run at RHIC¹³. The main source of this sensitivity to Δg comes from the Q^2 -evolutions of the inclusive g_1 structure function, but now with sea and valence distributions reasonably separated by semi-inclusive data in the global fit¹².

Jefferson Lab Hall A, with its high luminosity polarized ${}^3\text{He}$ target, has the unique advantage in providing high precision neutron asymmetry data in nucleon spin study. Recent Hall A data on inclusive A_{1n} and g_2^n measurements^{14,15} has improved previous world knowledge by an order of magnitude in each case. Such an improvement on semi-inclusive neutron asymmetries is also expected in this experiment, to be translated directly into knowledge of d -quark polarization. When compared with the expected deuteron data from semi-SANE experiment, a factor-of-three improvement

can be readily achieved in statistical uncertainties. This improved sensitivity will ultimately provide us with the discovery potential on the polarized sea asymmetry and gluon polarization, thus, put Jefferson Lab in head-to-head competition with RHIC-spin.

2 Physics Motivation

The principle goal of spin-dependent SIDIS experiments is to perform flavor decomposition of nucleon spin structure taking advantage of flavor tagging. In this section, we first express the SIDIS cross sections and asymmetries at leading order (LO) and summarize the HERMES results of “purity method” (more details in Appendix). After introducing the next-to-leading order cross sections, we summarize the NLO global QCD analysis method. We will then outline new methods of flavor decomposition: the Christova-Leader method at leading order and next-to-leading order and the leading order “fixed- z purity” method (details in Appendix). Theoretical models of polarized light sea asymmetry is summarized to motivate our measurement of $\Delta\bar{u} - \Delta\bar{d}$. Recent experimental evidence supporting the leading order naive x - z factorization are summarized at the end of this section. Throughout this proposal, SU(2) isospin symmetry and charge conjugation invariance are assumed and heavy quark contributions are neglected.

2.1 Beam-target double-spin asymmetries at leading order

At the leading order, the SIDIS process is factorized into a hard-scale quark scattering followed by a soft-scale hadronization. The “naive x - z factorization” assumption, on which the SMC and HERMES analysis were based, implies that the spin-independent (σ^h) and the spin-dependent ($\Delta\sigma^h$) cross sections follow:

$$\sigma^h(x, z) = \sum_f e_f^2 q_f(x) \cdot D_{q_f}^h(z), \quad \Delta\sigma^h(x, z) = \sum_f e_f^2 \Delta q_f(x) \cdot D_{q_f}^h(z), \quad (1)$$

where $x = Q^2/2M\nu$, $z = E_h/\nu$. The fragmentation functions $D_{q_f}^h(z)$ represent the probability that a quark f fragments into a hadron h .

Considering the beam and target polarization (P_B and P_T), and the dilution factor ($f^h = \sigma_{pol.N}^h/\sigma_{allN}^h$), which accounts for the unpolarized nucleons in the target, the double-spin asymmetry ³ for a longitudinally polarized beam on a longitudinally polarized target is :

$$A_{||}^h = f^h P_B P_T \cdot \mathcal{P}_{kin} \cdot A_{1N}^h, \quad (2)$$

the kinematic factor \mathcal{P}_{kin} is:

$$\mathcal{P}_{kin} = \mathcal{D} \cdot (1 + \gamma\eta) \cdot \frac{1 + R}{1 + \gamma^2}, \quad (3)$$

in which

$$\begin{aligned}\eta &= \frac{2\gamma(1-y)}{2-y}, & \mathcal{D} &= \frac{1-(1-y)\epsilon}{1+\epsilon \cdot R}, \\ \epsilon^{-1} &= 1 + 2(1+\nu^2/Q^2) \tan^2(\theta_e/2),\end{aligned}\quad (4)$$

\mathcal{D} is the virtual photon polarization, $R(x, Q^2) = \sigma_L/\sigma_T$ accounts for the longitudinal component of the virtual photon and $y = \nu/E_0$, $\gamma^2(x, Q^2) = 4M^2x^2/Q^2$. In the current fragmentation regime, the virtual photon asymmetry is defined as:

$$A_{1N}^h(x, Q^2, z) \equiv \frac{\Delta\sigma^h(x, Q^2, z)}{\sigma^h(x, Q^2, z)} = \frac{\sum_f e_f^2 \Delta q_f(x, Q^2) \cdot D_{q_f}^h(z, Q^2)}{\sum_f e_f^2 q_f(x, Q^2) \cdot D_{q_f}^h(z, Q^2)}. \quad (5)$$

In principle, the asymmetry A_{1N}^h depends on both variables x and z , its x -dependency comes from parton distributions and z -dependency comes from fragmentation functions. Accurate knowledge of the fragmentation functions is crucial in order to extract quark polarizations from the measured asymmetries. However, in some special combinations, if σ^h and $\Delta\sigma^h$ happen to have similar z -dependencies, as their ratio, the asymmetry will end up with a weak or even vanishing z -dependency. This type of cancellation can provide us with much cleaner observables to access quark polarizations without the complication of fragmentation functions. For example, Christova and Leader pointed out ⁹ that at the leading order, under the assumptions of SU(2) isospin symmetry and charge conjugation invariance, the fragmentation functions canceled exactly in the combined $h^+ \pm h^-$ double-spin asymmetries. Furthermore, if strange quark contribution can be neglected, the semi-inclusive asymmetry $A_{1N}^{\pi^+ \pm \pi^-}$ is reduced to the inclusive asymmetry A_{1N} . Even at the next-to-leading order, the z -dependence of $A_{1N}^{\pi^+ \pm \pi^-}$ is predicted to be very small ¹².

2.2 HERMES results from leading order purity method

The HERMES result of flavor decomposition ² is shown in Fig. 1. As expected, u -quarks are strongly polarized in the direction of proton spin, while d -quarks are polarized opposite to the proton spin. The sea quark polarizations are consistent with zero. Fig. 1 right panel shows the HERMES result of $x(\Delta\bar{u} - \Delta\bar{d})$ together with predictions of a broken SU(2)_f symmetry ^{16,17}. The data are consistent with an unbroken SU(2)_f sea symmetry.

The HERMES results left a lot of room for improvement, at least with respect to the statistics, especially on $\Delta\bar{u} - \Delta\bar{d}$. In addition, the validity and the stability of the leading order purity method needs to be independently verified. As pointed out by many authors, the issue of leading order factorization violation and the intrinsic uncertainties of the fragmentation Monte Carlo simulation need to be quantitatively addressed at the level appropriate to the sea contribution ⁹.

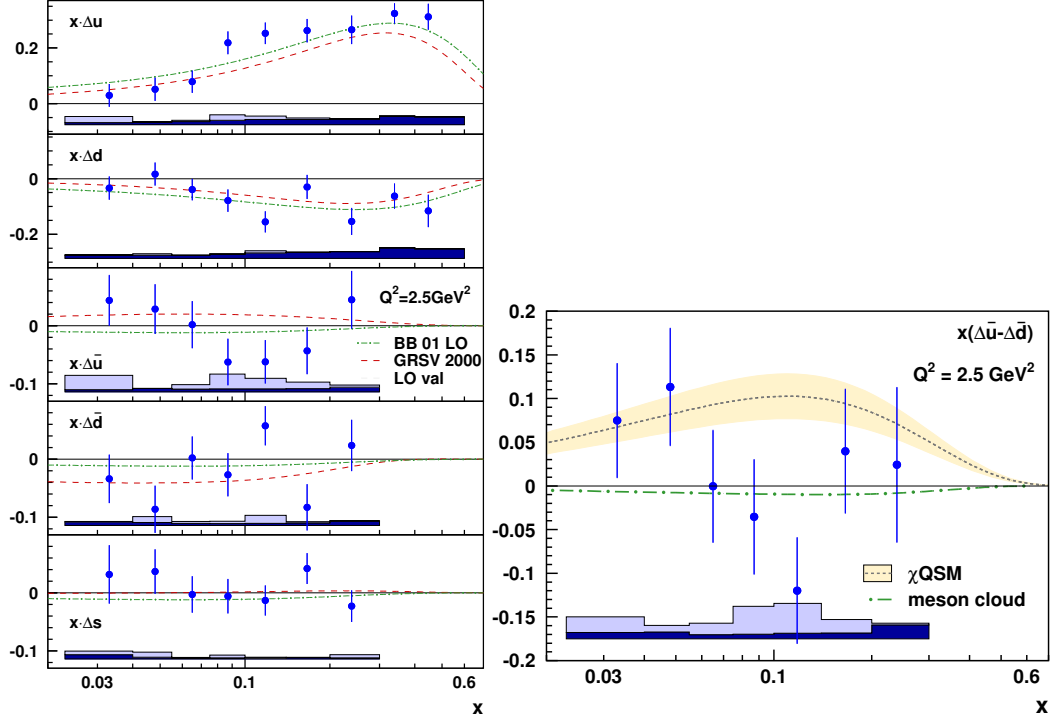


Figure 1: The HERMES result² of polarized quark distribution $x \cdot \Delta q(x)$ for u , \bar{u} , d , \bar{d} , and $s + \bar{s}$ versus x in comparison with two different parameterizations^{18,19} is shown on the left. The difference of the polarized light sea $x(\Delta \bar{u} - \Delta \bar{d})$ is shown on the right. The error bars are statistical, while the shaded bands at the bottom indicate the systematic uncertainties.

2.3 Neutron asymmetries are sensitive to Δd

Although the most recent HERMES spin-flavor decomposition data was on polarized protons and deuterons, one expects Δd to be better constrained by polarized ${}^3\text{He}$ data. The HERMES collaboration collected limited polarized ${}^3\text{He}$ target data in 1996, which formed the basis of the first flavor decomposition paper²⁰ in 1999.

From a simple argument based on e_q^2 -weighting and isospin symmetry, one expects the proton asymmetries are mostly sensitive to u -quark polarization while the neutron asymmetries are more sensitive to d -quark polarization. In Fig. 2, the fractional contribution of each quark flavor to the SIDIS cross sections σ_q/σ_{all} of proton (left panel) and neutron (right panel) are shown, that is:

$$\frac{\sigma_q}{\sigma_{all}} = \frac{e_q^2 \cdot q(x, Q^2) \cdot D_q^h(z, Q^2)}{\sum_f e_f^2 \cdot q_f(x, Q^2) \cdot D_f^h(z, Q^2)}. \quad (6)$$

Sensitivities of d -quark contribution to the neutron cross sections are clearly demonstrated.

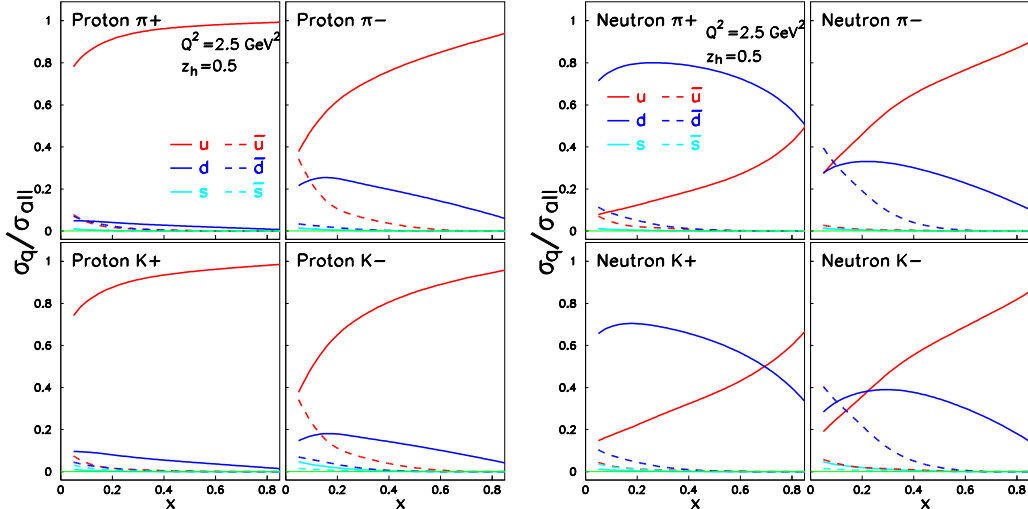


Figure 2: The left panel shows the proton SIDIS cross section as fractional contributions from each quark flavor at $Q^2 = 2.5 \text{ GeV}^2$ and $z_h = 0.5$. The right panel shows the case for a neutron.

2.4 SIDIS Cross sections at the next-to-leading order

The naive x - z factorization is no longer valid at the next-to-leading order when gluon diagrams in Fig. 3 are considered. However, the exact form of the NLO cross section has been well-known²¹. At NLO, the terms of $q(x) \cdot D(z)$ and $\Delta q(x) \cdot D(z)$ in Eq. 1 are added with the double convolutions of the type $q \otimes C \otimes D$ and $\Delta q \otimes \Delta C \otimes D$ in which C and ΔC are well-known Wilson coefficients²²:

$$[q \otimes C \otimes D](x, z) = \int_x^1 \frac{dx'}{x'} \int_z^1 \frac{dz'}{z'} q\left(\frac{x}{x'}\right) C(x', z') D\left(\frac{z}{z'}\right). \quad (7)$$

We define the short-hand notation:

$$qD + \frac{\alpha_s}{2\pi} q \otimes C \otimes D = q \left[1 + \otimes \frac{\alpha_s}{2\pi} C \otimes \right] D, \quad (8)$$

at NLO instead of Eq. 1, we have:

$$\begin{aligned} \sigma^h(x, z) &= \sum_f e_f^2 q_f \left[1 + \otimes \frac{\alpha_s}{2\pi} \mathcal{C}_{qq} \otimes \right] D_{q_f}^h \\ &+ \left(\sum_f e_f^2 q_f \right) \otimes \frac{\alpha_s}{2\pi} \mathcal{C}_{gg} \otimes D_G^h + G \otimes \frac{\alpha_s}{2\pi} \mathcal{C}_{gq} \otimes \left(\sum_f e_f^2 D_{q_f}^h \right), \end{aligned} \quad (9)$$

$$\begin{aligned} \Delta\sigma^h(x, z) &= \sum_f e_f^2 \Delta q_f \left[1 + \otimes \frac{\alpha_s}{2\pi} \Delta C_{qq} \otimes \right] D_{q_f}^h \\ &+ \left(\sum_f e_f^2 \Delta q_f \right) \otimes \frac{\alpha_s}{2\pi} \Delta C_{gg} \otimes D_G^h + \Delta G \otimes \frac{\alpha_s}{2\pi} \Delta C_{gq} \otimes \left(\sum_f e_f^2 D_{q_f}^h \right) \end{aligned} \quad (10)$$

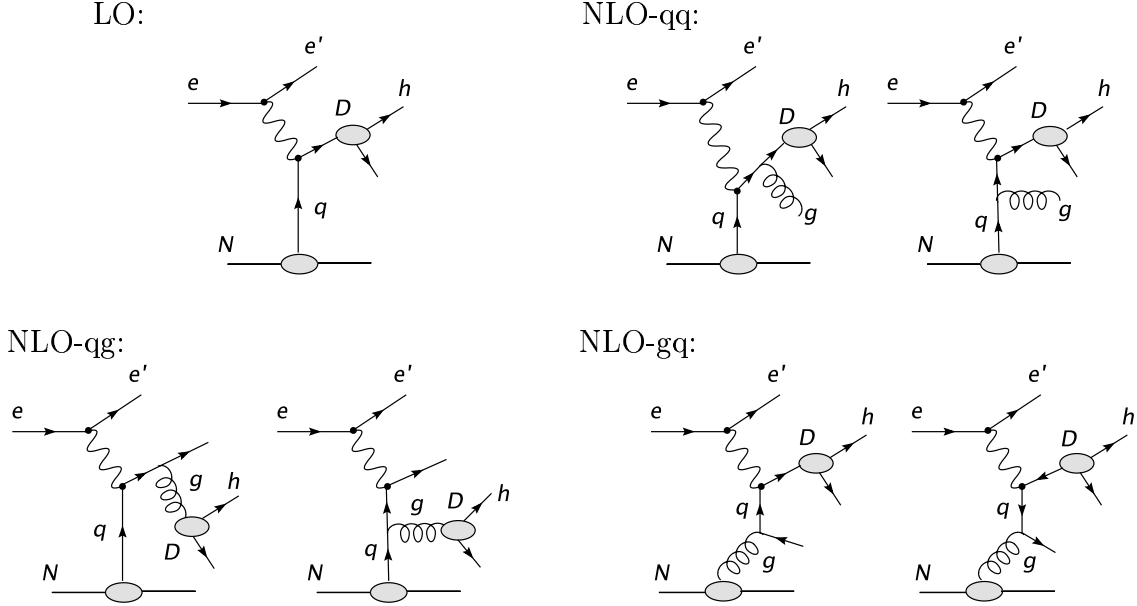


Figure 3: SIDIS diagrams at leading order (LO) and the next-to-leading order (NLO).

It is also well-known that in the Mellin- n space, the double-convolutions factorize into simple products under moments, and the parton distributions can be recovered by an inverse Mellin transformation with all moments of Wilson coefficients already calculated²³.

2.5 NLO global QCD analysis of DIS and SIDIS data

At the next-to-leading order, the cross sections in Eq. 5 are replaced by Eq. 9 and Eq. 10. Following the well established¹¹ formalism, tools of NLO QCD global fits, which include data sets from both inclusive and semi-inclusive reactions, have become available recently¹², and the uncertainties of the pPDF can be addressed in the global fits. With the new HERMES results, the polarized SIDIS data have a non-negligible weight in the combined global analysis, comparable to that of inclusive data. It helped to constrain the sea quark and gluon polarization complementing the information obtained from DIS. The NLO global fit¹² to the existing DIS and SIDIS data are shown in Fig. 28 in Appendix.

The precision data from this experiment, adding the neutron asymmetries to the world data, will serve as stringent constraints on pPDFs through NLO global fits. The impacts on pPDF moments are presented in the result section. Since the combined asymmetries $A_{1n}^{\pi^+ - \pi^-}$ are also measured in this experiment, the result of the NLO global fit can be cross checked with that from the NLO Christova-Leader method.

2.6 Methods of spin-flavor decomposition

Several independent methods can be used to achieve spin-flavor decomposition. At leading order, the result from the LO Christova-Leader method will be cross checked against the “fixed- z purity” method and the Monte Carlo purity method. Within the same data set, the naive x - z leading order factorization assumption can be tested quantitatively by comparing the combined asymmetry $A_{1n}^{\pi^+ + \pi^-}$ with the inclusive asymmetry A_{1n} . In this section, we give a brief outline of these flavor decomposition methods. More details are provided in Appendix.

LO Christova-Leader method to obtain $\Delta u_v(x)$, $\Delta d_v(x)$ and $\Delta \bar{u}(x) - \Delta \bar{d}(x)$

At the leading order, under isospin symmetry and charge conjugation invariance, the fragmentation functions cancel exactly in the combined asymmetry $A_{1N}^{\pi^+ + \pi^-}$. In addition, higher-twist terms in the fragmentation functions are also expected to be largely canceled⁹. In the quantities related to $\sigma^{\pi^+} - \sigma^{\pi^-}$, sea-quarks and gluons do not contribute at any QCD-order⁹.

From the Appendix, at leading order , for polarized protons, polarized deuterons and polarized neutrons^b (in ${}^3\text{He}$), we have:

$$A_{1p}^{\pi^+ - \pi^-}(\vec{p}) = \frac{\Delta\sigma_p^{\pi^+} - \Delta\sigma_p^{\pi^-}}{\sigma_p^{\pi^+} - \sigma_p^{\pi^-}} = \frac{4\Delta u_v - \Delta d_v}{4u_v - d_v}, \quad (11)$$

$$A_{1d}^{\pi^+ - \pi^-}(\vec{p} + \vec{n}) = \frac{\Delta\sigma_d^{\pi^+} - \Delta\sigma_d^{\pi^-}}{\sigma_d^{\pi^+} - \sigma_d^{\pi^-}} = \frac{\Delta u_v + \Delta d_v}{u_v + d_v}, \quad (12)$$

$$A_{1He}^{\pi^+ - \pi^-}(\vec{n} + 2\vec{p}) = \frac{\Delta\sigma_{He}^{\pi^+} - \Delta\sigma_{He}^{\pi^-}}{\sigma_{He}^{\pi^+} - \sigma_{He}^{\pi^-}} = \frac{4\Delta d_v - \Delta u_v}{7u_v + 2d_v}. \quad (13)$$

Measurements on three different targets will over-determine Δu_v and Δd_v . Proton and deuteron measurements are more sensitive to Δu_v , measurements on ${}^3\text{He}$ are more sensitive to Δd_v . One can re-write the last relation as:

$$(\Delta d_v - \frac{1}{4}\Delta u_v)_{LO} = \frac{1}{4}(7u_v + 2d_v) A_{1He}^{\pi^+ - \pi^-}. \quad (14)$$

This method involves helicity asymmetries on cross section differences. Kinematics need to be carefully chosen such that π^+ and π^- cross sections are reasonably different. Error propagation on $A_{1N}^{\pi^+ - \pi^-}$ make this method unfavorable when π^-/π^+ ratio approaches unity. Fig. 27 in Appendix illustrates this point by comparing the purity method with the Christova-Leader method using HERMES Data³.

We can obtain the leading order quantity $\Delta u_v - \Delta d_v$ from combinations of either proton and ${}^3\text{He}$ data or proton and deuteron data as:

$$(\Delta u_v - \Delta d_v)_{LO} = \frac{1}{5} \left[(4u_v - d_v) A_{1p}^{\pi^+ - \pi^-} - (7u_v + 2d_v) A_{1He}^{\pi^+ - \pi^-} \right], \quad (15)$$

^bAfter the effective neutron polarization (86.5%) in ${}^3\text{He}$ is taken into account and the correction corresponding to the small proton polarization (2.8%) is applied.

$$(\Delta u_v - \Delta d_v)_{LO} = \frac{1}{5} [2(4u_v - d_v)A_{1p}^{\pi^+ - \pi^-} - 3(u_v + d_v)A_{1d}^{\pi^+ - \pi^-}] . \quad (16)$$

On the other hand, constrained by the inclusive data, the flavor non-singlet quantity at all QCD order is:

$$\Delta q_3(x, Q^2) \equiv (\Delta u + \Delta \bar{u}) - (\Delta d + \Delta \bar{d}). \quad (17)$$

The polarized sea asymmetry at all QCD order is:

$$\Delta \bar{u} - \Delta \bar{d} = \frac{1}{2}\Delta q_3 - \frac{1}{2}(\Delta u_v - \Delta d_v). \quad (18)$$

At the leading order, we have:

$$\Delta q_3(x, Q^2)|_{LO} = 6 [g_1^p(x, Q^2) - g_1^n(x, Q^2)], \quad (19)$$

$$[\Delta \bar{u}(x) - \Delta \bar{d}(x)]_{LO} = 3[g_1^p(x) - g_1^n(x)] - \frac{1}{2}(\Delta u_v - \Delta d_v)|_{LO}. \quad (20)$$

NLO Christova-Leader method

At the next-to-leading order, under isospin symmetry and charge conjugation invariance, the NLO convolution terms become much simpler in quantities that are related to $\sigma^{\pi^+} - \sigma^{\pi^-}$. Since the gluon-related terms are identical for π^+ and π^- production, they drop out in the differences⁹:

$$A_{1p}^{\pi^+ - \pi^-}(\vec{p}) = \frac{(4\Delta u_v - \Delta d_v)[1 + \otimes(\alpha_s/2\pi)\Delta C_{qq}\otimes](D^+ - D^-)}{(4u_v - d_v)[1 + \otimes(\alpha_s/2\pi)\mathcal{C}_{qq}\otimes](D^+ - D^-)}, \quad (21)$$

$$A_{1d}^{\pi^+ - \pi^-}(\vec{p} + \vec{n}) = \frac{(\Delta u_v + \Delta d_v)[1 + \otimes(\alpha_s/2\pi)\Delta C_{qq}\otimes](D^+ - D^-)}{(u_v + d_v)[1 + \otimes(\alpha_s/2\pi)\mathcal{C}_{qq}\otimes](D^+ - D^-)}, \quad (22)$$

$$A_{1He}^{\pi^+ - \pi^-}(\vec{n} + 2\vec{p}) = \frac{(4\Delta d_v - \Delta u_v)[1 + \otimes(\alpha_s/2\pi)\Delta C_{qq}\otimes](D^+ - D^-)}{(7u_v + 2d_v)[1 + \otimes(\alpha_s/2\pi)\mathcal{C}_{qq}\otimes](D^+ - D^-)}. \quad (23)$$

in which Δu_v and Δd_v evolve as non-singlets and do not mix with sea-quark and gluon densities. Therefore, measurements of $A_{1N}^{\pi^+ - \pi^-}$ can determine Δu_v and Δd_v at the next-to-leading order without any consideration of gluon and sea distributions. The double-convolution terms in Eq. 21 are expected to introduce negligible z -dependency in $A_{1N}^{\pi^+ - \pi^-}$ at the kinematics of this experiment, as demonstrated in calculation of de Florian, Navarro and Sassot¹². The solution of Eq. 21 would follow an iterative procedure with the order from higher- x to lower- x points, since Δq_v at higher- x feed into the solution of lower- x in the convolution terms. Initial assumptions of Δq_v at high- x can be taken from a theoretical ansatz that respects positivity limits.

A well-defined procedure has been given²⁶ to obtain the moment $\Delta_1 u_v - \Delta_1 d_v$ directly from the measured asymmetries $A_{1N}^{\pi^+ - \pi^-}$ without first solving Eq. 21 point-to-point. It was further demonstrated²⁷ that, by applying the modification of Jacobian polynomial expansion method, the solutions of the first moment of pPDFs are stable even with data covering a limited x -range.

Cross check Δq_v with the upgraded RHIC

With the planned RHIC luminosity upgrade, Δq can be measured through W^\pm decays¹³. Since the Q^2 -evolutions of valence densities Δq_v are well understood in QCD, consistency cross checks can be made between JLab data at $\langle Q^2 \rangle = 2.2 \text{ GeV}^2$ and RHIC data at $Q^2 = M_W^2$.

The leading-order “fixed- z purity” method

The HERMES leading-order “purity” method can be much simplified if high statistics data are available at a well-defined z -value for all asymmetries. Instead of obtaining the “purity matrix” over a large z range as integrated quantities through a Monte Carlo, a well-localized “fixed- z purity” can be defined as described in detail in Appendix. The measured asymmetries are related with quark polarization through linear relations, for example on ${}^3\text{He}$:

$$A_{1He}^{\pi^+} = \frac{8\Delta u + 4\Delta d + \Delta \bar{u} + 2\Delta \bar{d} + (\Delta u + 2\Delta d + 8\Delta \bar{u} + 4\Delta \bar{d}) \lambda_\pi + 6\Delta s \xi_\pi}{8u + 4d + \bar{u} + 2\bar{d} + (u + 2d + 8\bar{u} + 4\bar{d}) \lambda_\pi + 6s \xi_\pi}, \quad (24)$$

where $\lambda_\pi(z) = D_\pi^-(z)/D_\pi^+(z)$ and $\xi_\pi(z) = D_s^\pi(z)/D_\pi^+(z)$ are ratios of fragmentation functions. These ratios are less uncertain than the fragmentation function themselves. The existing parameterizations²⁵ obtained from e^+e^- data provide reasonable accuracies to start with.

For a given x -bin, at a fixed z -value, each asymmetry measurement provides an independent constraint on a linear combination of quark polarizations. In addition to the semi-inclusive asymmetries A_{1N}^h , the well-known inclusive asymmetry A_{1p} and A_{1d} impose extra constraints on $\Delta u + \Delta \bar{u}$, $\Delta d + \Delta \bar{d}$ and $\Delta s + \Delta \bar{s} = 2\Delta s$.

2.7 $\Delta \bar{u} - \Delta \bar{d}$: the flavor asymmetry in the polarized sea

Fermilab experiment E866 reported measurements of the yield ratio of Drell-Yan muon pairs from an 800 GeV/c proton beam incident on hydrogen and deuterium^{28,29}. The data suggested a significantly asymmetric light sea quark distribution over an appreciable range in x ; the asymmetry \bar{d}/\bar{u} peaked around $x = 0.18$, as shown in Fig. 4. Furthermore, based on the E866 data and the CTEQ4M global-fit values of $\bar{u} + \bar{d}$, the values of $\bar{d}(x) - \bar{u}(x)$ were extracted, with the moment $\int_0^1 [\bar{d}(x) - \bar{u}(x)] dx = 0.118 \pm 0.012$. Many theoretical models, including the meson cloud model, the chiral-quark model, the Pauli-blocking model, the instanton model, the chiral-quark soliton model and the statistical model, have been proposed to explain the \bar{d}/\bar{u} asymmetry. These models can describe the \bar{d}/\bar{u} reasonably well. However, they all have difficulties explaining the \bar{d}/\bar{u} ratio at $x > 0.2$.

Since the unpolarized sea demonstrates a significant flavor asymmetry, one naively speculates a sizable flavor asymmetry also exists for the polarized sea in the same x -region. Indeed, many of models have specific implications for the spin structure

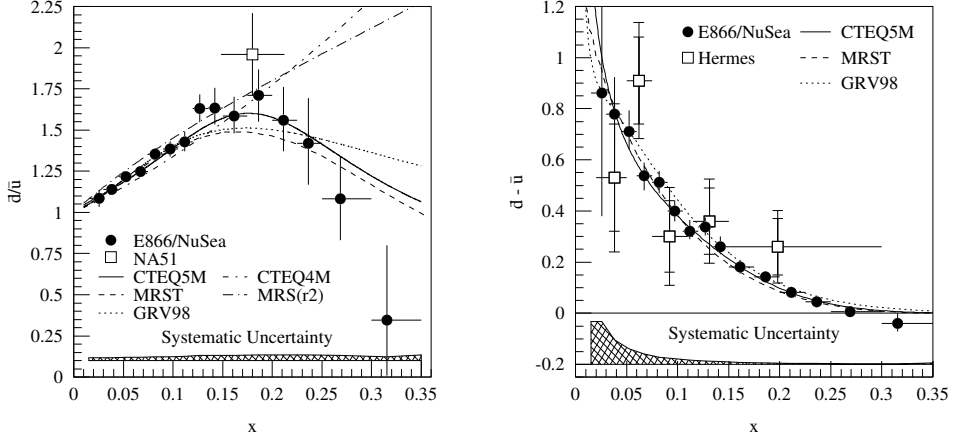


Figure 4: The Fermilab E866 results^{28,29}. The left plot shows the ratio \bar{d}/\bar{u} as a function of x , the right plot shows the extracted value of $\bar{d}(x) - \bar{u}(x)$ together with the HERMES semi-inclusive DIS results.

of the nucleon sea. For example, the Pauli-blocking model and the instanton model both predict a large asymmetry, $\int_0^1 [\Delta\bar{u}(x) - \Delta\bar{d}(x)]dx = \frac{5}{3} \cdot \int_0^1 [\bar{d}(x) - \bar{u}(x)]dx \approx 0.2$. In the chiral-quark soliton model, $\Delta\bar{u} - \Delta\bar{d}$ appears in leading-order (N_c^2) in a large N_c -expansion, while $\bar{d} - \bar{u}$ appears in the next-to-leading order (N_c). On the other hand, those meson cloud models which only include the π -meson predict $\Delta\bar{u} = \Delta\bar{d} = 0$ since the sea-quarks reside in a spin-0 π -meson. By considering a vector meson (ρ) cloud, non-zero sea polarization was predicted. A summary of theoretical predictions³⁰ of $I_\Delta = \int_0^1 [\Delta\bar{u}(x) - \Delta\bar{d}(x)]dx$ are given in Table. 1. If the flavor asymmetry of the polarized sea is indeed as large as the predictions of many models shown in Table. 1, it would imply that a significant fraction of the Bjorken sum, $\int_0^1 [g_1^p(x) - g_1^n(x)]dx$, comes from the flavor asymmetry of the polarized nucleon sea. The high statistics ${}^3\text{He}$ data from this experiment, together with the semi-SANE proton data, will provide us with the first opportunity to discover the asymmetry in the polarized sea.

2.8 The target single-spin asymmetry A_{UL}

As by-products, this experiment will also produce high statistics data on target single-spin asymmetry A_{UL}^n . Especially interesting is the $\sin 2\phi$ moment of A_{UL} , as shown in Eq. 25, is caused only by a non-vanishing chiral-odd Collins fragmentation function $H_1^{\perp q}$. CLAS eg1b data has observed a noticeable $A_{UL}^{\sin 2\phi}$, as shown in Fig. 5 together with the prediction⁴⁴ of Efremov *et al.*. A confirmation of such a non-zero single-spin asymmetry on the neutron is certainly rather interesting.

$$A_{UL}^{\sin 2\phi} = S_L \cdot \sin 2\phi \sum_q e_q^2 x h_{1L}^{\perp q}(x) \cdot H_1^{\perp q}(z), \quad (25)$$

In addition to the $\sin 2\phi$ moments, the $\sin \phi$ moments of A_{UL}^n , which are related to the neutron transversity and the higher-twist contributions, can also be extracted

Model	I_Δ prediction	Authors and References
Meson cloud (π -meson)	0	Eichten <i>et al.</i> ³¹ , Thomas ³²
Meson cloud (ρ -meson)	$\simeq -0.007$ to -0.027	Fries <i>et al.</i> ³³
Meson cloud ($\pi - \rho$ interference)	$= -6 \int_0^1 g_1^p(x) dx \simeq -0.7$	Boreskov <i>et al.</i> ³⁴
Meson cloud (ρ and $\pi - \rho$ interference)	$\simeq -0.004$ to -0.033	Cao <i>et al.</i> ¹⁷
Meson cloud (ρ -meson)	< 0	Kumano <i>et al.</i> ³⁵
Meson cloud ($\pi - \sigma$ interference)	$\simeq 0.12$	Fries <i>et al.</i> ³⁶
Pauli-blocking (bag model)	$\simeq 0.09$	Cao <i>et al.</i> ¹⁷
Pauli-blocking (ansatz)	$\simeq 0.3$	Gluck <i>et al.</i> ³⁷
Pauli-blocking	$= \frac{5}{3} \int_0^1 [\bar{d}(x) - \bar{u}(x)] dx \simeq 0.2$	Steffens ³⁸
Chiral-quark soliton	0.31	Dressler ³⁹
Chiral-quark soliton	$\simeq \int_0^1 2x^0.12[\bar{d}(x) - \bar{u}(x)] dx$	Wakamatsu <i>et al.</i> ⁴⁰
Instanton	$= \frac{5}{3} \int_0^1 [\bar{d}(x) - \bar{u}(x)] dx \simeq 0.2$	Dorokhov ⁴¹
Statistical	$\simeq \int_0^1 [\bar{d}(x) - \bar{u}(x)] dx \simeq 0.12$	Bourrely <i>et al.</i> ⁴²
Statistical	$> \int_0^1 [\bar{d}(x) - \bar{u}(x)] dx \simeq 0.12$	Bhalerao ⁴³

Table 1: A summary³⁰ of theoretical predictions of $I_\Delta = \int_0^1 [\Delta\bar{u}(x) - \Delta\bar{d}(x)] dx$.

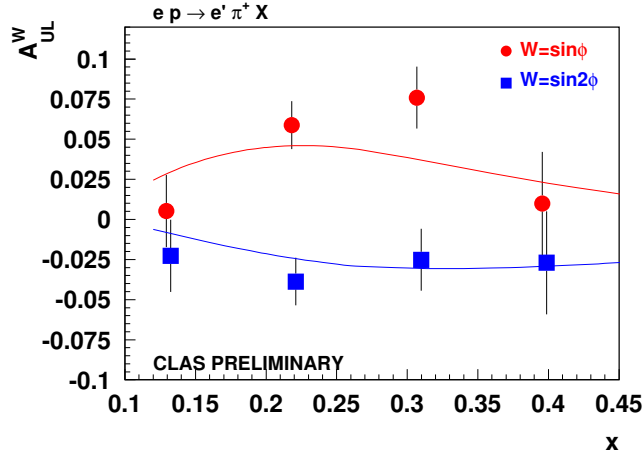


Figure 5: Azimuthal moment of target single-spin asymmetry $A_{UL}^{\sin\phi}$ and $A_{UL}^{\sin 2\phi}$ from CLAS EG1b $\vec{p}(e, e'\pi^+)X$ data⁵. The kinematic cuts are $0.5 < z < 0.8$ and $W' > 1.1$ GeV. Curves are from A. Efremov *et al.*⁴⁴

to help better understand the recent HERMES proton transversity data⁴⁵ and the upcoming data from the Hall A neutron transversity experiment⁴⁶ (E03-004).

2.9 Recent JLab data suggests leading order naive $x - z$ factorization

The quark-hadron duality argument of Close and Isgur⁴⁷ suggests that leading order factorization might work at the Jefferson Lab energies. Recent cross section data also supports such a claim. In Fig. 6 left, the preliminary Hall C E00-108 cross section ratio⁶ between proton and deuteron for $\sigma^{\pi^+} + \sigma^{\pi^-}$ is plotted vs. z . The measured ratio turns out to be rather flat between $0.45 < z < 0.70$ and agrees well with the factorization prediction (solid line). This z -independent behavior, a direct consequence of the leading order factorization assumption, indicates that information of quark distribution is well-preserved in SIDIS reactions at JLab energies, and the higher-twist effects are either small or canceled out in cross section ratios. The lack of resonance structures at $z < 0.70$ ($W' > 1.5$ GeV) indicates that the contributions from exclusive resonance production are not large when $W' > M_\Delta$, confirming earlier observations of Cornell experiments^{48,49} at $E_0 = 11$ GeV.

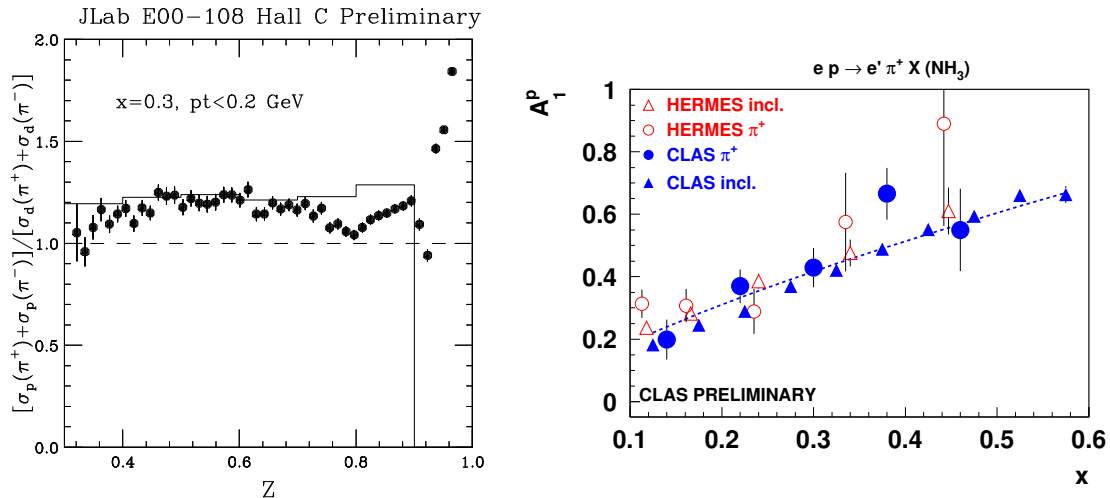


Figure 6: Left: preliminary cross section ratios from E00-108 experiment. The ratio of proton and deuteron ($e, e'\pi$) cross section at $x = 0.3$ are shown to agree with a SIDIS Monte Carlo simulation (solid line). Right: CLAS $A_{1p}^{\pi^+}$ data compared with HERMES data, the inclusive A_{1p} asymmetries are also plotted for comparison.

The existing asymmetry data also suggests leading order $x-z$ factorization at 6 GeV. In the right panel of Fig. 6, clear agreement of $A_{1p}^{\pi^+}$ between HERMES and CLAS data is shown. In addition, the semi-inclusive asymmetries clearly agree with the inclusive asymmetry A_{1p} , indicating the strong domination of current-quark fragmentation in the semi-inclusive data. The CLAS data corresponding to $\langle Q^2 \rangle = 1.77$ GeV² and a rather low missing mass cut of $W' > 1.1$ GeV.

3 The Proposed Measurement

3.1 Overview

We plan to study the $\vec{n}(\vec{e}, e'h)X$ reactions ($h = \pi^+$ and π^- , K^+ and K^- as by-products) with a longitudinally polarized ${}^3\text{He}$ target in Hall A with a 6 GeV polarized electron beam. Relative yields will be determined for $(e, e'\pi^+)$ and $(e, e'\pi^-)$ reactions such that the combined asymmetries $A_{1N}^{\pi^+\pm\pi^-}$ can be constructed in addition to the various double-spin asymmetries A_{1n}^h . As shown in Fig. 7, the left-HRS

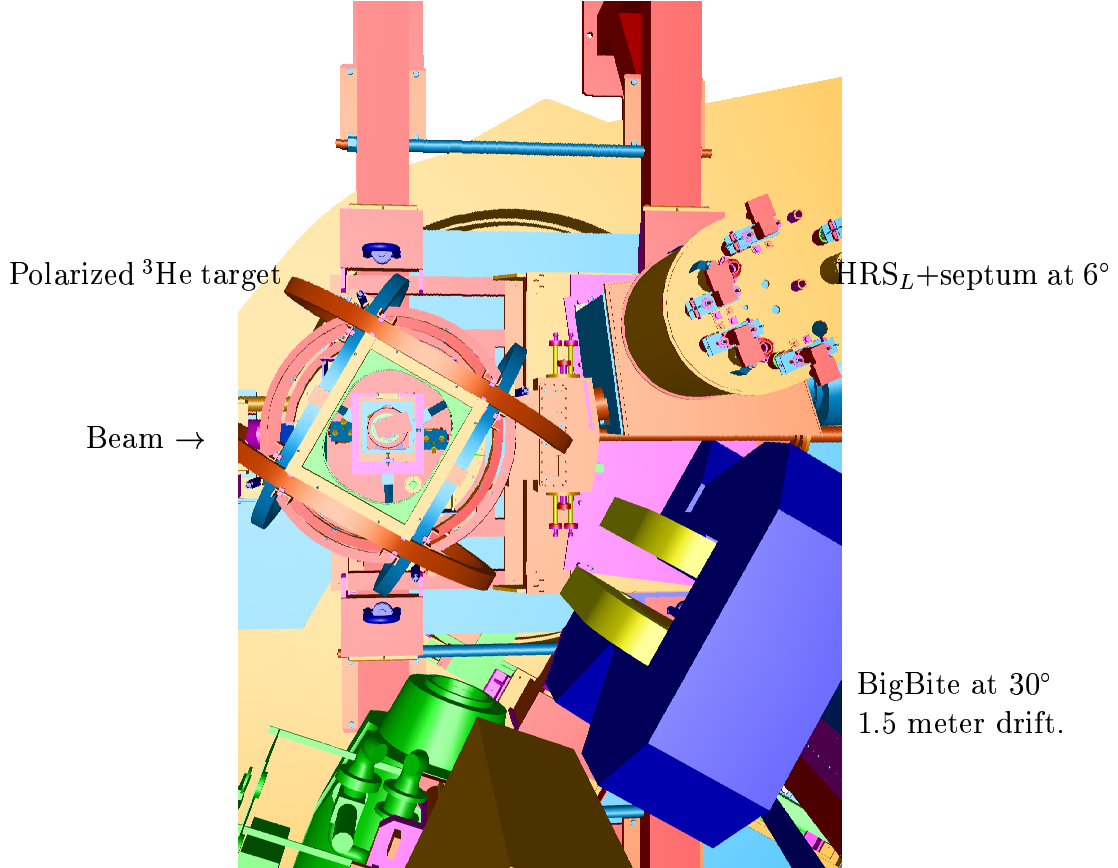


Figure 7: A top view of the Hall A instruments near the interaction points for this experiment. Beam comes in from the left side. Left septum coupled with HRS is at 6° , the BigBite spectrometer is shown on beam right at 30° with a drift distance of 1.5 meter. The right HRS is parked at 110° .

spectrometer with its septum magnet will be located at 6° as the hadron arm detector at a central momentum of 2.40 GeV/c for either positive or negative polarity. For the electron arm, we will use the recently constructed BigBite spectrometer. The BigBite detector package will be in exactly the same configuration as in the G_{En} experiment⁵⁰ (E02-013) and the neutron transversity experiment⁴⁶ (E03-004). Since this experiment is a coincidence experiment, and the HRS spectrometer can be used for interaction vertex reconstruction, most of the complications associated

with the BigBite wire chamber track reconstruction can be eliminated, in contrast to the case of the G_{En} experiment. In addition, when a tight coincidence timing cut is further required we expect that the majority of the background tracks and random hit events in the BigBite wire chambers can be easily eliminated.

3.2 Kinematics and phase space

The definitions of the kinematics variables are the following: Bjorken- x , which indicates the fractional momentum carried by the struck quark, $x = Q^2/(2\nu M_N)$, M_N is the nucleon mass. The momentum of the outgoing hadron is p_h and the fraction of the virtual photon energy carried by the hadron is: $z = E_h/\nu$. W is the invariant mass of the whole hadronic system and W' is the invariant mass of the hadronic system without the detected hadron. We have:

$$W^2 = M_N^2 + Q^2 \left(\frac{1}{x} - 1 \right),$$

$$W'^2 = (M_N + \nu - E_\pi)^2 - |\vec{q} - \vec{p}_\pi|^2. \quad (26)$$

We have chosen to cover the highest possible W with a 6 GeV beam, $2.31 < W < 3.07$ GeV, corresponds to $0.12 < x < 0.41$ and $1.21 < Q^2 < 3.12$ (GeV/c) 2 . We chose to detect the leading hadron which carries $z \approx 0.5$ of the energy transfer to strongly favor the current fragmentation regime. The value of missing mass W' is chosen to be as high as possible (1.57~2.35 GeV) to avoid contributions from resonance structures. The central kinematic values for each x -bin are listed in Table 2.

E' GeV	θ_e deg.	x	W GeV	Q^2 GeV 2	θ_q deg.	z_π	p_h GeV/c	W'_π GeV	η_{cm}^π	x_F^π
$\theta_h = 6.0^\circ$										
0.75	30.0	0.122	3.07	1.21	4.0	0.46	2.40	2.35	2.06	0.45
1.15	30.0	0.203	2.85	1.85	6.6	0.50	2.40	2.12	2.19	0.49
1.55	30.0	0.298	2.60	2.49	9.5	0.54	2.40	1.86	1.81	0.53
1.95	30.0	0.413	2.31	3.12	12.7	0.59	2.40	1.57	1.32	0.57

Table 2: The nominal kinematics for the central BigBite angle of 30° and HRS angle of 6.0° . The HRS momentum setting ($p_{HRS} = 2.40$ GeV/c) and the central z and W' values are listed. Data of all x -bins will be collected simultaneously. Higher x -bins ($x > 0.41$) are not listed.

The phase space coverage is obtained from a detailed Monte Carlo simulation which includes realistic septum and HRS spectrometer models, detector geometry and target geometry. The HRS spectrometer with its septum magnet has a nominal solid angle of 5.0 msr and a momentum bite of $\pm 4.5\%$. The BigBite spectrometer at 1.5 meter drift distance has an effective solid angle of 64 msr. The phase space covered in this experiment is shown in Fig. 8. We only plot the phase space corresponding to $E' < 2.15$ GeV. By setting the hadron arm at 6° , directly along

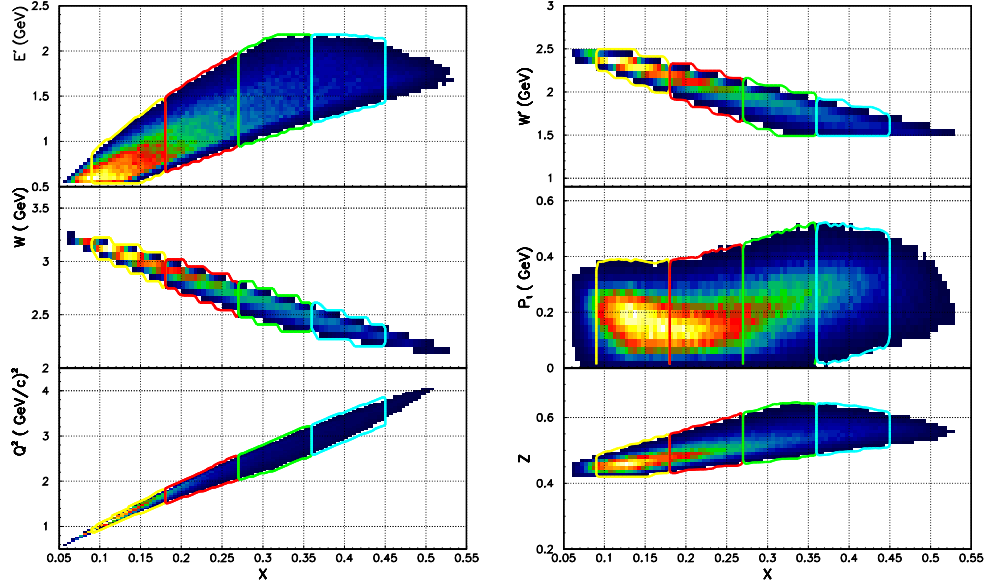


Figure 8: Left panel: the phase space coverage in (Q^2, x) and (W, x) planes for each x -bin. Phase space beyond $E' = 2.15$ GeV is not plotted. Right panel: phase space coverage in (W', x) , (p_t, x) and (z, x) planes. The actual kinematic coverage is wider compared with the nominal values listed in Table 2.

the average \vec{q} direction, we cover the azimuthal angle as unbiased as possible. The hadron azimuthal angle ($\phi_{\pi q}$) and polar angle ($\theta_{\pi q}$) coverage relative to the \vec{q} direction is shown in Fig. 9.

The left panel in Fig. 10 illustrates the two-dimensional plot⁵¹ of z vs η_{CM} for $W = 2.5$ GeV, where the center-of-mass rapidity $\eta_{CM} = \frac{1}{2} \ln \frac{E+P_L^*}{E-P_L^*}$ is defined in the center-of-mass frame. When $z^\pi \approx 0.5$ is required, the current and target fragmentation regimes are reasonably well separated. The right panel of Fig. 10 illustrates the phase space of η_{cm}^π vs x_F^π in this experiment. The separation in center-of-mass rapidity η_{cm}^π in this experiment is comparable to the regularly used Berger's criterion for separation of current and target fragmentation⁵².

3.3 The experimental observables

The beam and target double-spin asymmetries can be obtained directly from the number of events (N^+ and N^-) observed corresponding to each beam helicity, corrected by the luminosity ratio $\mathcal{L}^+/\mathcal{L}^-$:

$$A_{^{1He}}^h = \frac{1}{f^h P_B P_T \mathcal{P}_{kin}} \cdot \frac{N^+ - N^- \cdot \frac{\mathcal{L}^+}{\mathcal{L}^-}}{N^+ + N^- \cdot \frac{\mathcal{L}^+}{\mathcal{L}^-}} \quad (27)$$

Since the CEBAF electron beam flips its helicity at a rate of 30 Hz, and a beam

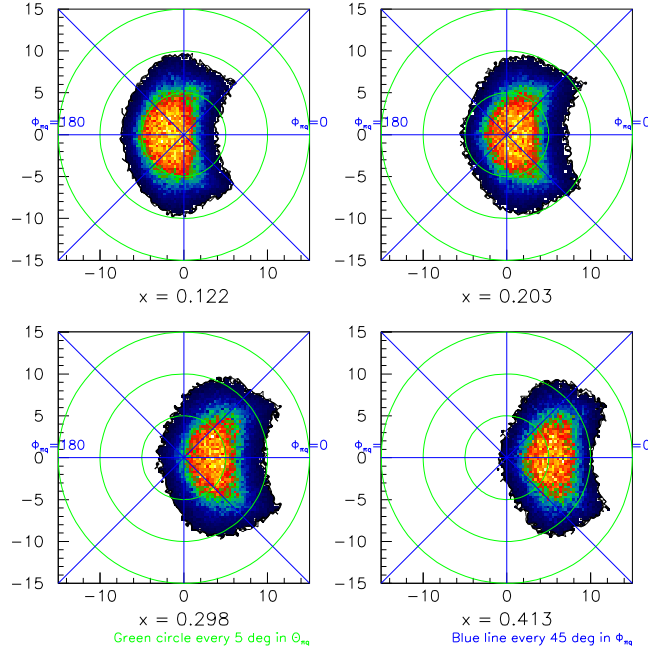


Figure 9: The hadron azimuthal angle ($\phi_{\pi q}$) and polar angle ($\theta_{\pi q}$) coverage for each x -bin. The \vec{q} vector goes into the page at the middle of each plot.

charge feed back system continuously controls the beam charge asymmetry Q^+/Q^- below 100 ppm, practically, we have $\mathcal{L}^+/\mathcal{L}^- = 1$ for this experiment. The dilution factors f^h will be measured by comparing spectra from polarized target runs with that of the reference cell runs with Hydrogen, Deuterium, Helium-3 and Nitrogen gas. These dilution factors are expected to be measured to $\delta f/f \leq 2\%$ within a relatively short time. The uncertainties on the double-spin asymmetries δA_{1He}^h is dominated by the statistical uncertainties of $\delta A_{||}^h$ with the dilution factor uncertainties play a minor role.

The combined asymmetry $A_{1He}^{\pi^+\pm\pi^-}$ needs the cross section ratio $r = \sigma_{He}^{\pi^-}/\sigma_{He}^{\pi^+}$ as an extra input:

$$A_{1He}^{\pi^+\pm\pi^-} = \frac{\Delta\sigma_{He}^{\pi^+} \pm \Delta\sigma_{He}^{\pi^-}}{\sigma_{He}^{\pi^+} \pm \sigma_{He}^{\pi^-}} = \frac{A_{1He}^{\pi^+} \pm A_{1He}^{\pi^-} \cdot r}{1 \pm r}. \quad (28)$$

For this experiment, we have roughly $r = \sigma_{He}^{\pi^-}/\sigma_{He}^{\pi^+} = 0.52 \sim 0.70$. The error propagation follows:

$$(\delta A_{1He}^{\pi^+\pm\pi^-})^2 = \frac{1}{(1 \pm r)^2} \left[(\delta A_{1He}^{\pi^+})^2 + r^2 (\delta A_{1He}^{\pi^-})^2 + (A_{1He}^{\pi^-})^2 (\delta r)^2 + (A_{1He}^{\pi^+\pm\pi^-})^2 (\delta r)^2 \right]. \quad (29)$$

The value of r can be easily determined statistically to $|\delta r|/r \leq 2.0\%$ in this experiment. The systematic uncertainty should also be below 2.0%, since only count

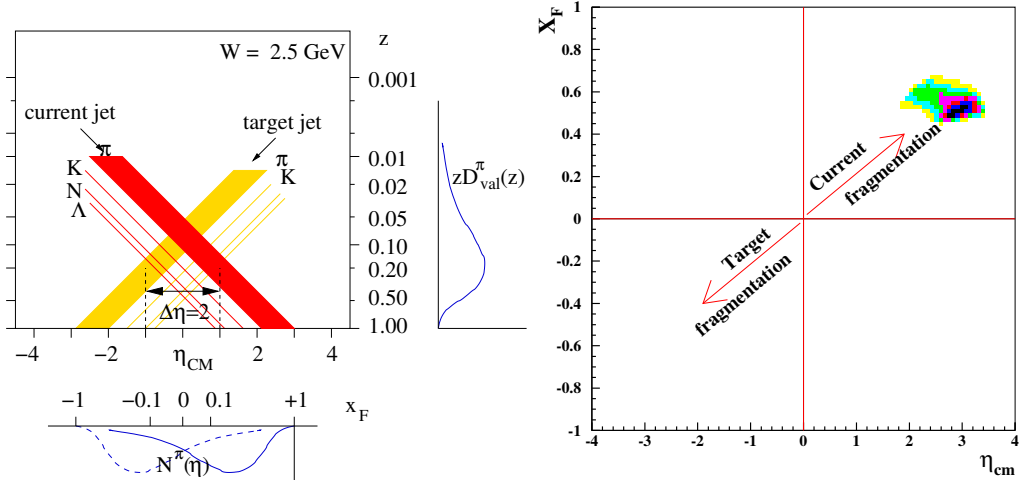


Figure 10: The center-of-mass rapidity gap for $W = 2.5$ GeV is illustrated in the left panel, above $z = 0.50$ the current and target fragmentation regime is separated by $\Delta\eta_{CM} = 3.8$. A typical fragmentation function is shown with $z = E_\pi/\nu$ and $x_F = p_L^\pi/|\vec{q}|$. The center-of-mass rapidity η_{cm}^π vs x_F^π plot for this experiment is shown on the right.

ratios over exactly the same phase spaces are involved. In addition, the uncertainty of r is always modulated by the asymmetries, thus, the first two terms dominate in Eq. 29.

The target single-spin asymmetry A_{UL} will be obtained from the number of events (N^\rightarrow and N^\leftarrow) observed for the target polarization along or against the beam direction, corrected by the luminosity difference $\mathcal{L}^\rightarrow/\mathcal{L}^\leftarrow$. The phase space coverage of the azimuthal angle $2\phi_{q\pi}$ is shown in Fig 11. The luminosity will be monitored by various spectrometer singles rates. In addition, frequent target spin-flips, roughly once every half hour, are expected to further eliminate the uncertainties on the luminosity ratio in A_{UL} measurements. The beam helicity is averaged over.

$$A_{UL}^h = \frac{1}{fP_B \mathcal{P}_{kin}^{UL}} \cdot \frac{N^\rightarrow - N^\leftarrow \cdot \frac{\mathcal{L}^\rightarrow}{\mathcal{L}^\leftarrow}}{N^\rightarrow + N^\leftarrow \cdot \frac{\mathcal{L}^\rightarrow}{\mathcal{L}^\leftarrow}} \quad (30)$$

3.4 The electron arm: BigBite

The BigBite spectrometer will be located at 30° and at a drift distance of 1.50 meter, instead of the 1.1 meter drift in E02013. The BigBite detector package will be exactly the same as in E02013. Three sets of wire chambers will be used to provide tracking information followed by a pre-shower, scintillator and shower assembly to provide trigger and particle ID for the electrons. The BigBite dipole magnet will be set at the full current with $|\vec{B}| = 1.2$ T. Charged particles with momentum less than 0.2 GeV/c will be eliminated as shown in Fig. 12.

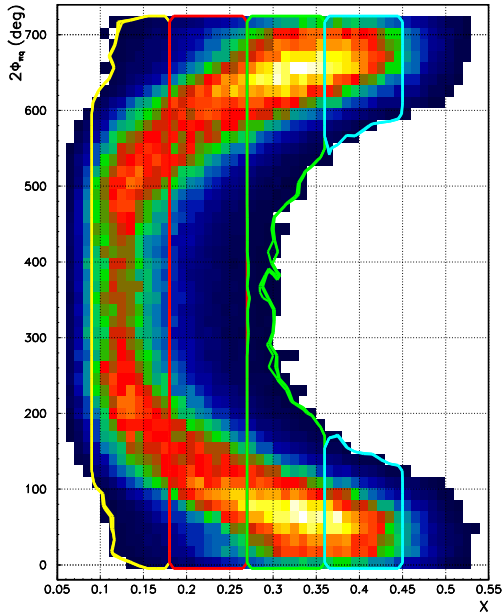


Figure 11: Hadron azimuthal angle $2\phi_{q\pi}$ coverage for each x -bin.

The BigBite collaboration has already built three sets of wire chambers, each has U-U', V-V' and X-X' planes. The sense wire separation is 2.0 cm, corresponding to a drift cell size of 1.0 cm and a maximum drift time of 100 ns. A GEANT Monte Carlo simulation⁵⁰ has shown that with a typical chamber resolution of 200 μm , the momentum resolution ($\delta p/p$) is $\approx 2\%$. The angular resolution is 3.0 mrad in each direction, causing a few MeV uncertainty in P_\perp reconstruction. The vertex resolution will be better than 2.0 cm along the beam. Since this experiment does not seek to resolve any structure in the final states, and the SIDIS events will be grouped in rather large x -bins, the momentum and angular resolutions designed for E02-013 will be adequate for this experiment.

The electron's particle ID will be provided by a set of pre-shower and shower detectors. The pre-shower blocks are made of TF-5 lead glass, $10 \times 10 \times 37 \text{ cm}^3$ each, covering an active area of $210 \times 74 \text{ cm}^2$, with 10 cm (3 r.l.) along the particle's direction. The total absorption shower blocks are made of TF-2 lead glass, $8.5 \times 8.5 \times 34 \text{ cm}^3$ each, covering an active area of $221 \times 85 \text{ cm}^2$, with 34 cm (13 r.l.) along the particle's direction. The total depth of lead glass is enough to contain electron showers with energies up to 10 GeV, with an energy resolution of $8.0\%/\sqrt{E}$. A typical pion rejection factor of 100:1 is expected. Based on Hall C SOS spectrometer data taken at a similar kinematics, the expected singles π^-/e^- ratio will be less than 60:1 in this experiment.

The BigBite acceptance as a function of particle momentum and interaction point is shown in Fig. 13. An average solid angle of 64 msr is expected, with the vertical angle $\Delta\theta_t = \pm 240$ mrad ($\pm 13.7^\circ$) and the horizontal angle $\Delta\phi_t = \pm 67$ mrad ($\pm 3.8^\circ$).

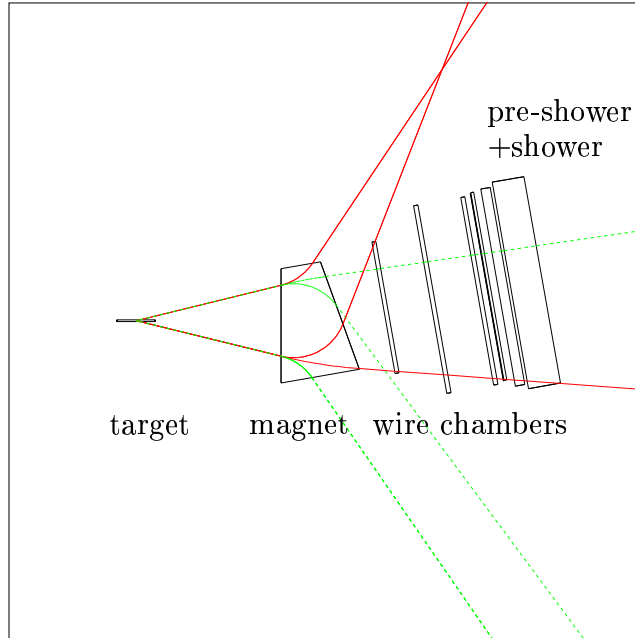


Figure 12: Typical charged particle trajectories through the BigBite spectrometer and its detector package. Particles with $p = 0.2$ and 1.8 GeV/c are shown starting from vertical angles of $\theta_t = \pm 240$ mrad. The upward bending tracks are negatively charged particles, and the downward bending tracks are positively charged particles. The location of wire chambers, trigger scintillator planes, pre-shower and shower lead glass arrays are also indicated.

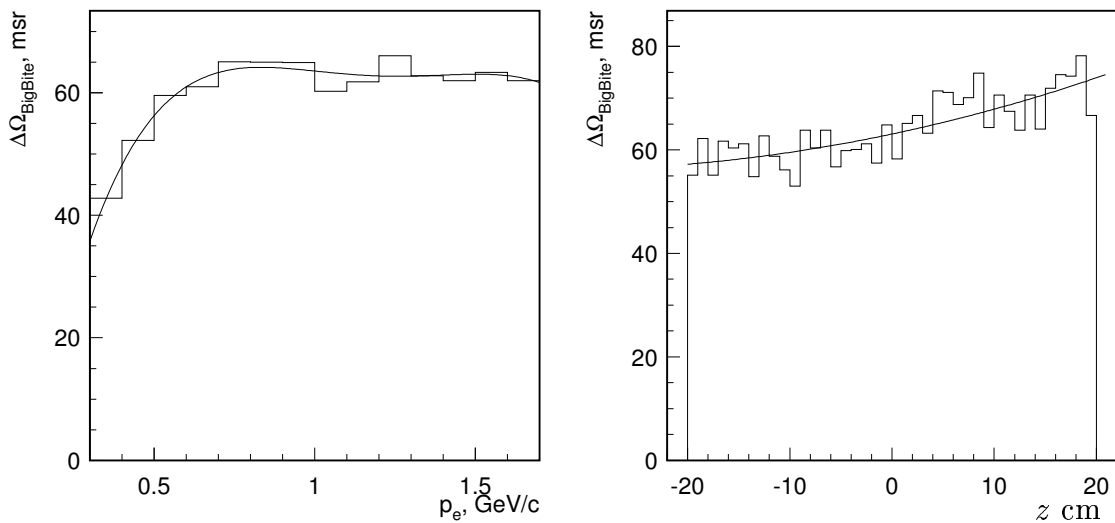


Figure 13: BigBite acceptance as a function of particle momentum (left) and as a function of interaction point (right).

Single particle background and track reconstruction in BigBite

The background rates in the BigBite detectors are calculated using the Monte Carlo simulation code GDINR⁵³. For particles with momentum above 200 MeV/c, the integrated electron rate is less than 100 kHz, the π^- rate is less than 150 kHz. The positron rate is less than 1 kHz, the π^+ rate is less than 300 kHz. The majority of the charged particle background comes from protons with $p > 200$ MeV/c ($T_p > 21$ MeV). Such a proton rate of 3 MHz is comparable to the situation of E02-013, and can be tolerated by the wire chambers.

The low energy photon background in BigBite is the major concern of this experiment. According to the Monte Carlo, the total photon rate could reach 50~100 MHz, similar to the situation of E02-013. Since the maximum drift time in MWDC is 100 ns, the average multiplicity on each plane could reach 5~10 hits per trigger. This relatively high level of chamber activity could cause a large number of candidate tracks for a single arm experiment, for an $(e, e'n)$ type measurement, such as in E02-013. In a coincidence measurement, however, in which the trigger involves the timing coincidence of two charged particles from two spectrometers, high resolution vertex information from HRS_L on a long target helps in reducing the tracking ambiguity in BigBite, especially when the HRS_L arm is clean. For BigBite tracking, in the transverse direction, a straight line between the HRS_L reconstructed vertex and the center of shower at the calorimeter serves as the starting point of track reconstruction. In the dispersive direction, the location of a shower also helps in track selection. Furthermore, the reconstructed particle momentum has to be consistent with the energy deposited in the calorimeter.

By taking the BigBite to a 1.5 meter drift distance, extra space is available before the magnet to construct shielding and to install collimators. Parasitic background tests for the BigBite spectrometer have been planned in Hall A during 2005, and improvements on the detectors and shielding are expected. We expect that, by the time E02-013 starts taking production data in late 2005, shielding improvements of BigBite will make the background level acceptable to this experiment.

In addition, the Hall A Penta-quark collaboration is planning to build an aerogel Cherenkov detector (30 cm in thickness) to be added in front of the pre-shower detector. Charged pion background below 400 MeV/c will be eliminated, if the detector is constructed before this experiment, introducing only a small reduction in the solid angle.

3.5 The hadron arm: HRS+septum

The HRS_L detectors, with two aerogel Cherenkov detectors and a RICH detector, will provide particle identification information for this experiment. The aerogel detectors A1 (n=1.015) and A2 (n=1.055) will provide a clean $\pi/K/p$ separation, their momentum thresholds are shown in Fig. 14. In addition, the RICH detector will also provide independent $\pi/K/p$ separation. The lead-glass detectors will provide a clean π^-/e^- separation.

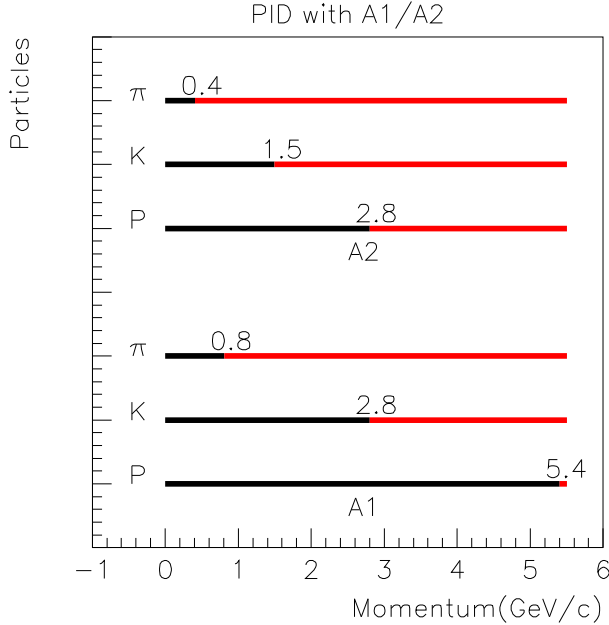


Figure 14: The Cherenkov thresholds for pions, kaons and protons in the two aerogel detectors.

Based on data collected during the small angle GDH experiment (E97-110) we estimate that in this experiment the single π^- rate in HRS_L will be at the few kHz level, the single electron rate will also be at the kHz level.

The optics of $HRS+septum$ system has been well-studied in several experiments for both the positive and the negative polarities, and for both one septum and two septa operations. Single arm acceptance Monte Carlo was shown to reproduce data reasonably well for E97-110. Beam steering tests have also been carried out in June 2005 with a 4-pass beam, and it was shown to be not an issue for septum operation with either polarities.

3.6 Trigger and offline event selection

A coincidence time window of 50 ns will be enough to form the coincidence trigger. Trajectory corrected time-of-flight resolution is expected to be about 2 ns. The raw accidental coincidence rate will be less than 500 Hz. After the BigBite calorimeter ADC cut and the HRS_L PID cut, accidental coincidence events are not expected to survive at any significant level. Two-arm vertex consistency cut is expected to further eliminate the accidental events, by an additional factor of 10, if there are any left. The true ($e, e'\pi$) coincidence event rate is expected to be at 1 Hz level when all x -bins are summed over.

3.7 The polarized ^3He target

The Hall A polarized ^3He target has been successfully used for experiments E94-010 and E95-001 in 1998-1999, E99-117 and E97-103 in 2001, E97-110 and E01-012 in 2003. The polarized ^3He target uses optically pumped rubidium vapor to polarize ^3He nuclei via spin exchange. For a 40 cm long target with target density corresponding to 10 atm at 0°C, average in-beam target polarization is about 42% with a beam current of 15 μA . Two kinds of polarimetry, NMR and EPR (Electron-Paramagnetic-Resonance), are used to measure the polarization of the target. The relative uncertainty in the target polarization measurement is $\pm 2.5\%$.

The target cell in this experiment will have a conical shape on the front side, similar to the cells used in experiment E97-110 in 2003, as shown in Fig. 15. The special shaped cell minimize energy loss and multiple scattering for particles emerging at 6°.

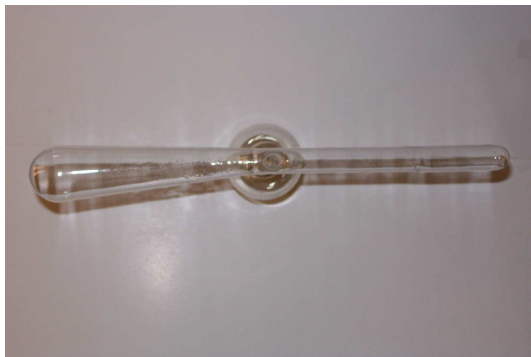


Figure 15: The conically shaped target cell as used in the Hall A small angle GDH experiment.

Effects of BigBite and septum magnetic field

The BigBite magnet will be 1.5 meters away from the target center. Its fringe field might cause a field gradient in the target region. We plan to use a field clamp, similar to the design of E02-013, to suppress the field gradient. Recent operation experience during experiment E97-110, in which the polarized target was used in conjunction with the septum magnet, suggested that target polarization loss due to AFP flip during a polarization measurement was rather small. It turned out that the two correction coils initially installed to reduce the field gradient were never used during E97-110. Later in 2005, BigBite fringe field at the target location will be mapped to verify that the current BigBite field clamp satisfies the design specifications. As a backup plan, correction coils will be installed just as in E97-110. A typical plot of on-line EPR and NMR target polarization measurements from E97-110 is shown in Fig. 16. The polarized target system has gone through upgrades and improvements constantly. All the numbers we used for our rate estimate are based on achieved performance.

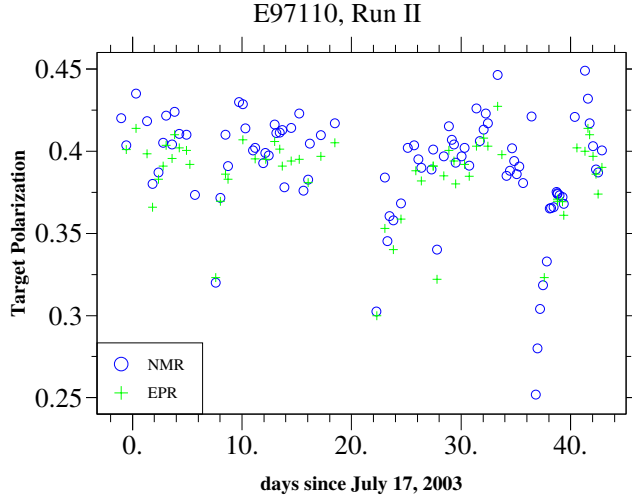


Figure 16: On-line EPR and NMR target polarization measurements during experiment E97-110 (calibrations are not final).

4 Event Rate Estimate and Statistical Uncertainties

4.1 Cross section and rate estimate

The estimation of the coincidence cross sections has the following inputs:

- The inclusive $p(e, e')$ and $n(e, e')$ cross sections. Deep-inelastic cross sections for ${}^3\text{He}$ are assumed to be the sum of the two-protons plus one neutron, neglecting the nuclear effects in the intermediate x -region.
- Parameterizations of the fragmentation functions D_π^+ , D_π^- and D_s^π for quark to pion fragmentation, D_K^+ , D_K^- and D_d^K for quark to kaon fragmentation.
- A model of the transverse momentum distributions of pion and kaon as fragmentation products.

The inclusive deep inelastic (e, e') cross section can be expressed in the quark parton model as:

$$\frac{d^2\sigma}{d\Omega dE'} = \frac{\alpha^2(1 + (1 - y)^2)}{sxy^2} \frac{E'}{M_N \nu} \sum_{q,\bar{q}} e_q^2 f_1^q(x), \quad (31)$$

where $s = 2E M_N + M_N^2$. The unpolarized quark distribution functions $f_1^q(x)$ and $f_1^{\bar{q}}(x)$ are taken from the CTEQ5M global fits⁵⁴. The semi-inclusive $(e, e'h)$ cross section relates to the quark fragmentation function $D_q^h(z)$ and the total inclusive cross section σ_{tot} through:

$$\frac{1}{\sigma_{tot}} \frac{d\sigma(e, e'h)}{dz} = \frac{\sum_{q,\bar{q}} e_q^2 f_1^q(x) D_q^h(z)}{\sum_{q,\bar{q}} e_q^2 f_1^q(x)}. \quad (32)$$

For the quark to pion fragmentation functions $D_\pi^+(z)$ and $D_\pi^-(z)$, we follow the parameterization²⁵ of KKP to obtain the sum of $D_\pi^+(z) + D_\pi^-(z)$. For the ratio $D_\pi^-(z)/D_\pi^+(z)$, which is important to the error propagation^c of $A_{^3He}^{\pi^+ - \pi^-}$, we use a fit⁵⁶ to the HERMES data⁵⁷: $D_\pi^-/D_\pi^+ = (1-z)^{0.084}/(1+z)^{1.984}$. Fragmentation functions D_s^π , D_K^+ , D_K^- and D_d^K in the KKP parameterization are used.

Existing data indicate that the fragmented products follow a Gaussian-like distribution in transverse momentum. For the $N(e, e'\pi)X$ reaction, recent HERMES preliminary data[?] showed that the transverse momentum (P_\perp) distribution for both π^+ and π^- follow the form of $e^{(-aP_\perp^2)}$ with $a = 3.76 \text{ (GeV/c)}^{-2}$, corresponding to an average quark transverse momentum of $\langle P_\perp^2 \rangle = 0.26 \text{ (GeV/c)}^2$. Charged kaon transverse momentum distributions are also found to be similar[?]. We used this distribution and realistic spectrometer acceptances in a Monte Carlo simulation to estimate the count rates. The issue of hadron decay is also considered in the rate estimation. The typical survival factors for π^\pm and K^\pm of 2.40 GeV/c momentum are 0.83 and 0.25 correspondingly, after a flight-path of 26.0 m through septum magnet and HRS.

4.2 Statistical uncertainties on raw asymmetries

The event rates, total number of events in each bin, the statistical uncertainties of the raw asymmetries are listed in Table 3 for the $(e, e'\pi)$ and $(e, e'K)$ reactions. We have assumed a beam current of 15 μA , beam polarization of 85%, a target length of 40 cm with a ${}^3\text{He}$ gas pressure of 10 atm and a target polarization of 42%.

4.3 Statistical uncertainties on physics asymmetries and Δd_v

The expected statistical uncertainties on ${}^3\text{He}$ physics asymmetries $A_{^3He}^h$ and $A_{^3He}^{\pi^\pm \pi^\mp}$ are listed in Table 4.

Physics asymmetries on ${}^3\text{He}$ are translated into neutron asymmetries $A_{^1n}^h$ and listed in Table 5 together with the corresponding dilution factors. An effective neutron polarization of 86.5% in ${}^3\text{He}$ ground state has been taken into account.

Statistical uncertainties on polarized parton distribution $\delta \left[x(\Delta d_v - \frac{1}{4}\Delta u_v) \right]_{CL}$ according to the leading order Christova-Leader (CL) method, uncertainty propagation following Eq. 11, are listed in Table 6.

^c If we use the fragmentation functions of Kretzer *et al*⁵⁵, as in the original semi-SANE experiment proposal (E04-113), $D_\pi^-(z) = 0.217z^{-1.805}(1-z)^{2.037}$ and $D_\pi^+(z) = 0.689z^{-1.039}(1-z)^{1.241}$, statistical uncertainties on $A_{^3He}^{\pi^+ - \pi^-}$, Δd_v and $\Delta \bar{u} - \Delta \bar{d}$ will be reduced by 20% \sim 30%. More details are given in Appendix.

$(e, e'\pi^\pm)$ rates and total number of events on ${}^3\text{He}$ target:

$\langle x \rangle$	$\langle z_\pi \rangle$	R^{π^+} Hz	R^{π^-} Hz	N^{π^+} k	N^{π^-} k	$P_B P_T \mathcal{P}_{kin}$	$\delta A_{ }^{\pi^+}$ %	$\delta A_{ }^{\pi^-}$ %
0.122	0.46	0.42	0.29	470.	198.	0.416	0.15	0.22
0.203	0.50	0.27	0.17	301.	114.	0.370	0.18	0.30
0.298	0.54	0.14	0.08	160.	55.	0.329	0.25	0.43
0.413	0.59	0.05	0.03	61.	19.	0.292	0.41	0.72

$(e, e'K^\pm)$ rates and total number of events on ${}^3\text{He}$ target:

$\langle x \rangle$	$\langle z_K \rangle$	R^{K^+} Hz	R^{K^-} Hz	N^{K^+} k	N^{K^-} k	$P_B P_T \mathcal{P}_{kin}$	$\delta A_{ }^{K^+}$ %	$\delta A_{ }^{K^-}$ %
0.122	0.47	0.062	0.037	70.	25.	0.416	0.38	0.63
0.203	0.51	0.038	0.019	43.	13.	0.370	0.48	0.89
0.298	0.55	0.021	0.008	23.	6.	0.329	0.65	1.33
0.413	0.60	0.008	0.003	9.	2.	0.292	1.03	2.35

Table 3: Pion and kaon event rates (R^h), the total number of events (N^h), the product of kinematic factor, beam and target polarization ($P_B P_T \mathcal{P}_{kin}$), the expected statistical uncertainties of raw asymmetry ($\delta A_{||}^h$) are listed. Data of all x -bins will be collected simultaneously.

4.4 Systematic uncertainties

Systematic uncertainty of A_{1He}^h and A_{1n}^h

Knowledge of target polarization and dilution factor dominates the systematic uncertainty of A_{1n}^h . The effects of radiative corrections will be treated in a Monte Carlo simulation following the procedures of the HERMES analysis ², which found that the systematic uncertainties introduced by this procedure are negligible. Kinematic smearing will also be treated following the procedure of the HERMES analysis.

Major systematic uncertainties in double-spin asymmetries A_{1n}^h :

Uncertainty in target polarization $\delta P_T/P_T$:	$\pm 2.5\%$ relative
Uncertainty in beam polarization $\delta P_B/P_B$:	$\pm 2.0\%$ relative
Helicity correlated beam charge uncertainty $\delta(Q_+/Q_-)$:	$\ll 10^{-4}$ absolute
Radiative correction and smearing:	$\pm 1.5\%$ relative
Dilution factor $\delta f/f$:	$\pm 2.5\%$ relative
Total systematic uncertainty of A_{1n}^h	$\pm 4.3\%$ relative

The systematic uncertainties of $A_{1He}^{\pi^+\pm\pi^-}$ are propagated from $A_{1He}^{\pi^+}$ and $A_{1He}^{\pi^-}$ while assuming a systematic uncertainty of $\delta r/r = 2.0\%$ in Eq. 29. Similar to the case of the semi-SANE experiment, the statistical uncertainties dominate in the error propagation of this experiment.

$\langle x \rangle$	$\delta A_{1He}^{\pi^+}$ %	$\delta A_{1He}^{\pi^-}$ %	$\delta A_{1He}^{K^+}$ %	$\delta A_{1He}^{K^-}$ %	$\delta A_{1He}^{\pi^+\pi^-}$ %	$\delta A_{1He}^{\pi^-\pi^-}$ %
0.122	0.35	0.54	0.91	1.52	0.30	1.76
0.203	0.49	0.80	1.30	2.40	0.43	1.93
0.298	0.76	1.29	1.99	4.05	0.68	2.52
0.413	1.39	2.47	3.54	8.04	1.25	4.02

Table 4: The statistical uncertainties of double-spin asymmetry $A_{1He}^h(\vec{n} + 2p)$ for ${}^3\text{He}$ in which the effective neutron polarization in the ${}^3\text{He}$ ground state (86.5%) has been taken into account.

$\langle x \rangle$	f^{π^+}	f^{π^-}	$\delta A_{1n}^{\pi^+}$ %	$\delta A_{1n}^{\pi^-}$ %	f^{K^+}	f^{K^-}	$\delta A_{1n}^{K^+}$ %	$\delta A_{1n}^{K^-}$ %
0.122	0.276	0.333	1.47	1.87	0.285	0.336	3.69	5.23
0.203	0.242	0.320	2.35	2.89	0.253	0.320	5.94	8.66
0.298	0.206	0.301	4.28	4.97	0.216	0.290	10.65	16.14
0.413	0.173	0.293	9.24	9.72	0.180	0.262	22.75	35.45

Table 5: The expected statistical uncertainties of the double-spin asymmetry A_{1n}^h and the corresponding dilution factors.

Effective nucleon polarization in ${}^3\text{He}$

Effective nucleon polarization in ${}^3\text{He}$ for deep-inelastic scattering gives:

$$g_1^{{}^3\text{He}} = P_n g_1^n + 2P_p g_1^p \quad (33)$$

where $P_n(P_p)$ is the effective polarization of the neutron (proton) inside ${}^3\text{He}$ ⁶⁰. These effective nucleon polarizations $P_{n,p}$ can be calculated using ${}^3\text{He}$ wave functions constructed from N-N interactions, and their uncertainties were estimated using various nuclear models^{59,60,61,62}, giving

$$P_n = 0.86_{-0.02}^{+0.036} \quad \text{and} \quad P_p = -0.028_{-0.004}^{+0.009}. \quad (34)$$

The small proton effective polarization (2.8%) causes small offsets in the ${}^3\text{He}$ asymmetries, compared to that from a free neutron. The uncertainties associated with

$\langle x \rangle$	xu_v	xd_v	$\delta [x(\Delta d_v - \frac{1}{4}\Delta u_v)]_{CL}$
0.122	0.596	0.317	0.021
0.203	0.703	0.327	0.027
0.298	0.644	0.256	0.032
0.413	0.459	0.150	0.035

Table 6: The expected statistical uncertainties of $\delta [x(\Delta d_v - \frac{1}{4}\Delta u_v)]_{CL}$ according to the leading order Christova-Leader (CL) method. Values of $xu_v(x)$ and $xd_v(x)$ from CTEQ are also listed.

this small offset are even smaller when considering that the corresponding proton asymmetries are better known and will be improved with the Hall C semi-SANE data.

At $x = 0.1 \sim 0.4$, especially around $x = 0.3$, the nuclear EMC effect becomes rather small, as has been demonstrated on many different nucleus.

π - N final state interaction

Since pions carry no spin, πN final state interactions will not introduce asymmetries in $A_{^1He}^h$. Effect of π - N final state interaction will come through the dilution factors. By measuring the leading pions at 2.4 GeV/c, where the π - N total cross sections are reasonably flat, effects of FSI are minimized. A detailed π - N re-scattering calculation⁶³ confirmed that the modifications to the cross section are rather small at this kinematics.

Target fragmentation and vector meson production

In principle, intermediate ρ production processes are part of the fragmentation process and should not be subtracted from the SIDIS cross sections. Furthermore, due to the charge conjugation, the effect of intermediate ρ^0 production is canceled in observables related to $\pi^+ - \pi^-$. Therefore, the Christova-Leader method of flavor decomposition is not sensitive to ρ production.

At a high- z setting of this experiment ($z \approx 0.5$), target fragmentation contamination is expected to be small, as has been shown by the HERMES LUND based Monte Carlo simulation. In addition, in the $\pi^+ - \pi^-$ yield target fragmentation contributions are mostly canceled.

Corrections from non-vanishing A_\perp^n

Since the target polarization is along the beam direction, not exactly along the virtual photon direction θ_{γ^*} , measurements of $A_{||}$ should in principle be corrected by a small contribution from A_\perp in order to obtain the physics asymmetry $A_{^1N}^h$. In this experiment, we have $\sin \theta_{\gamma^*} \approx 0.1$, therefore, the uncertainty associated with this correction is of the order $0.1 \times (\delta A_\perp^n)$.

In the published HERMES and SMC data, the corrections from A_\perp were neglected based on the observation that in inclusive DIS $g_2(x)$ turned out to be rather small. The residual effect of non-vanishing g_2 (or A_\perp) in SIDIS has been included in the estimation of systematic uncertainties in the HERMES case. The contribution to the fractional systematic uncertainties on $A_{^1N}^h$ was estimated to be 0.6% for proton and 1.4% for deuteron.

In principle, about 10% of beam time of this experiment should be allocated for transverse target runs such that the exact corrections of A_\perp^n can be applied. However, we chose not to request this extra beam time based on the following considerations:

- The leading order contribution in A_{\perp} (or A_{LT} in Mulders' notation) is modulated by an angular dependence of $\cos(\phi_s - \phi_h)$. When a reasonable range of ϕ_h is covered, as in this experiment, the averaged contribution from A_{\perp} will most likely to be washed out.
- Aside from the angular modulation, A_{\perp} was predicted to be at the 10% level for the proton in bag-model calculations (Mulders, Yuan). Assuming A_{\perp}^n is at the similar level, the correction to A_{1n}^h will be at 1% level for this experiment, much less than the statistical uncertainties.
- The value of A_{\perp} will likely to be determined to much better than 10% in the next few years. HERMES experiment has already collected data on a transversely polarized proton target with polarized positron beam, from which the beam-target double-spin asymmetry A_{\perp}^p can be extracted with reasonable precision. The approved Hall C SANE experiment, which runs with a transversely polarized proton target (NH_3), will also provide information on A_{\perp}^p if coincidence data is taken in a parasitic mode. The Hall A neutron transversity experiment (E03-004), with a transversely polarized ${}^3\text{He}$ target, will provide information on A_{\perp}^n at a similar kinematics.

Based on the above consideration, we feel confident that even without dedicated transverse target runs the systematic uncertainties associated with A_{\perp}^n correction will be much less compared to the statistical uncertainties of this experiment.

Systematic uncertainty of Δq , $\Delta\bar{u} - \Delta\bar{d}$

The consistency of Δq obtained from several leading order independent methods of flavor decomposition will serve as cross-checks of the systematic uncertainties in this experiment. The HERMES analysis shown that the uncertainties in the fragmentation function dominated the systematic uncertainties in the flavor decomposition of the LO purity method, introducing uncertainties of $0.02 \sim 0.06$ in the value of the extracted $\Delta u/u$ and $\Delta d/d$. The uncertainties introduced by the unpolarized PDFs and R are found to be very small. Since we will only need the ratios of the fragmentation functions as inputs for flavor decomposition, we would expect a smaller systematic uncertainties compared to that of the HERMES analysis.

Part of the systematic uncertainties due to the knowledge^{19,14} of $g_1^p(x)$ and $g_1^n(x)$ ($\delta g_1^p = 0.0059$, $\delta g_1^n = 0.0057$) are also included in obtaining $\delta(\Delta\bar{u} - \Delta\bar{d})_{LO}$ in Fig. 20. The SANE experiment⁵⁸ in Hall C is expected to improve the world knowledge of $g_1^p(x)$ significantly. The inclusive data from this experiment will also provide a high statistical data set for extracting $g_1^n(x)$.

5 Beam time request, hardware costs and installation time needed

5.1 Beam time request

The beam time request are listed in detail in Table 7. The relative time between π^+ and π^- runs are chosen to minimize the uncertainty of $A_{^{3}\text{He}}^{\pi^+ - \pi^-}$ for the $x = 0.203$ bin. We request 576 hours (24 days) of total beam time, of which 500 hours is for beam on the polarized ^{3}He target. A considerable amount of overhead time (60 hours total) is requested. This overhead time can be shared between activities such as Möller measurements, unpolarized target runs, and target polarization measurements, as has been done in the past during other Hall A polarized ^{3}He target experiments. Major target related down times can also be arranged to coincide with the scheduled accelerator maintenance activities in order to save overhead time.

	Time- h^+ hour	Time- h^- hour
Production	312	188
Beam on polarized target		500
Optics check and detector shakedown		16
Overhead, Möller runs and reference cell runs.		60
Total Time Request		576 (24 days)

Table 7: Details of the beam time request.

5.2 Hardware costs and installation time needed

All major hardware components required in this experiment, including the target, spectrometers and detectors are either already standard Hall A equipments or about to become the standard Hall A equipments. The BigBite spectrometer together with its electron-detection package is scheduled to be commissioned in late 2005 for the G_{En} experiment. This proposal has no additional requirement on the BigBite detectors beyond its expectation for the G_{En} experiment.

The existing septum magnet support table, originally designed to accommodate two septa magnets, need to be re-made for single septum support to avoid interference with the BigBite spectrometer. The cost of the new table is \$12k. The front legs of the BigBite support frame, originally designed to be moved around the pivot, need to be modified to accommodate the interaction point's 80 cm upstream shift introduced by the use of septum magnet. The cost of this modification is \$18k. The overall hardware cost of this experiment, including installation cost, will be \$50-60k, make it a relatively modest experiment at Jefferson Lab..

The overall installation time needed for this experiment is estimated to be between four to six weeks. Installation of the standard polarized ${}^3\text{He}$ target in conjunction with the left septum magnet can be accomplished within two to three weeks, as has been demonstrated during previous operations. The installation time needed for the BigBite spectrometer, depends on the sequence of experiments, could be one to two weeks.

6 The Expected Results

6.1 Double spin asymmetries A_{1He}^h and A_{1n}^h

The expected statistical accuracies of semi-inclusive double-spin asymmetries are shown in Fig. 18 as functions of x . HERMES and SMC deuteron asymmetries are translated into neutron asymmetries, according to the leading order cross section assumption, and plotted as a comparison.

6.2 Flavor decomposition of quark polarization and the impacts to NLO global fits

$\Delta d_v(x)$ from the leading-order Christova-Leader method

Statistical accuracies of $x\Delta d_v$ from this experiment, according to the leading order Christova-Leader method, are plotted in Fig. 19 together with the projected uncertainties of the Semi-SANE experiment. The published data from HERMES, which used the purity method and included inclusive asymmetry data, are also plotted. When the HERMES data were analyzed following the Christova-Leader method, dramatic increase in statistical uncertainties can not be avoid due to the unfavorable cross section ratio of $\sigma^{\pi^-}/\sigma^{\pi^+}$ in the HERMES kinematics (see Fig. 27 in Appendix). The SMC data, which assumed symmetric sea polarization, are shown. For the error propagation of both semi-SANE and this experiment in Fig. 19, we have assumed cross section ratios following the HERMES fragmentation function. Error reduction of $20 \sim 30\%$ is expected if the KLC fragmentation function ratios are assumed, as shown in Fig. 30 in Appendix.

$\Delta\bar{u}(x) - \Delta\bar{d}(x)$ from the leading-order Christova-Leader method

When combined with the expected semi-SANE proton data, this experiment is very sensitive to the polarized sea asymmetry $\Delta\bar{u}(x) - \Delta\bar{d}(x)$, as shown in Fig. 20 together with several theory predictions. The much improved sensitivity will provide us with the first opportunity to make the discovery of an asymmetric polarized sea.

Leading-order quark polarization of all flavor

The “fixed- z purity” method of flavor decomposition will be used in a combined analysis of semi-SANE data (p,d) and data from this experiment. The two-experiments have almost identical kinematics, strong constraints on the fragmentation function

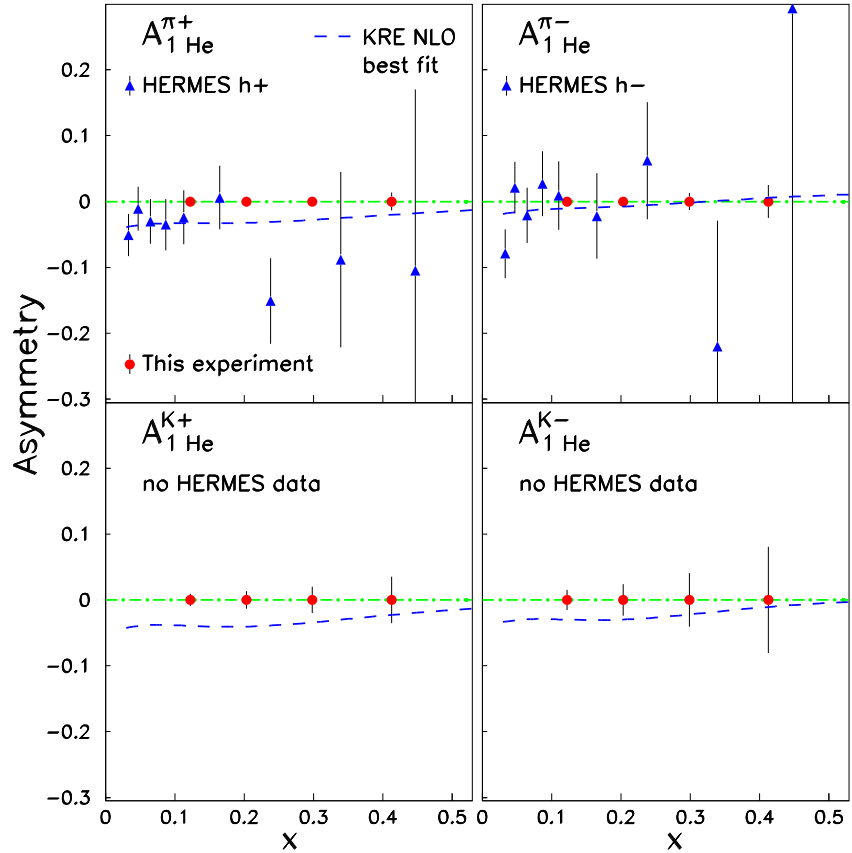


Figure 17: The expected statistical accuracy of pion and kaon semi-inclusive physics asymmetries on ${}^3\text{He}$. The HERMES 1997 data on a polarized ${}^3\text{He}$ target obtained without hadron PID² are also shown as a comparison. The next-to-leading order “best fit” results corresponding to the Kretzer fragmentation function (KRE) is show as dashed curves.

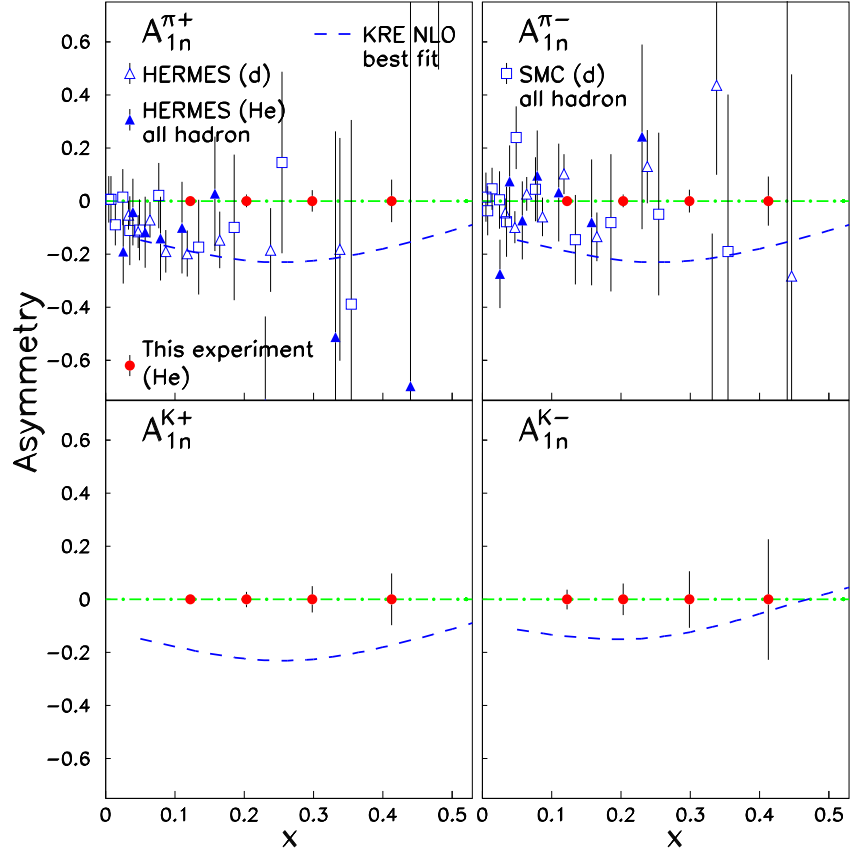


Figure 18: The expected statistical accuracy of asymmetries corresponding to “a free neutron target” $A_{1n}^{\pi+}$, $A_{1n}^{\pi-}$, A_{1n}^{K+} and A_{1n}^{K-} as functions of x . HERMES results² on the deuteron target are also shown. The next-to-leading order “best fit” results corresponding to the Kretzer fragmentation (KRE) is show as dashed curve. A comparison with the projected semi-SANE (d) error bars is shown in Fig. 29 in the Appendix.

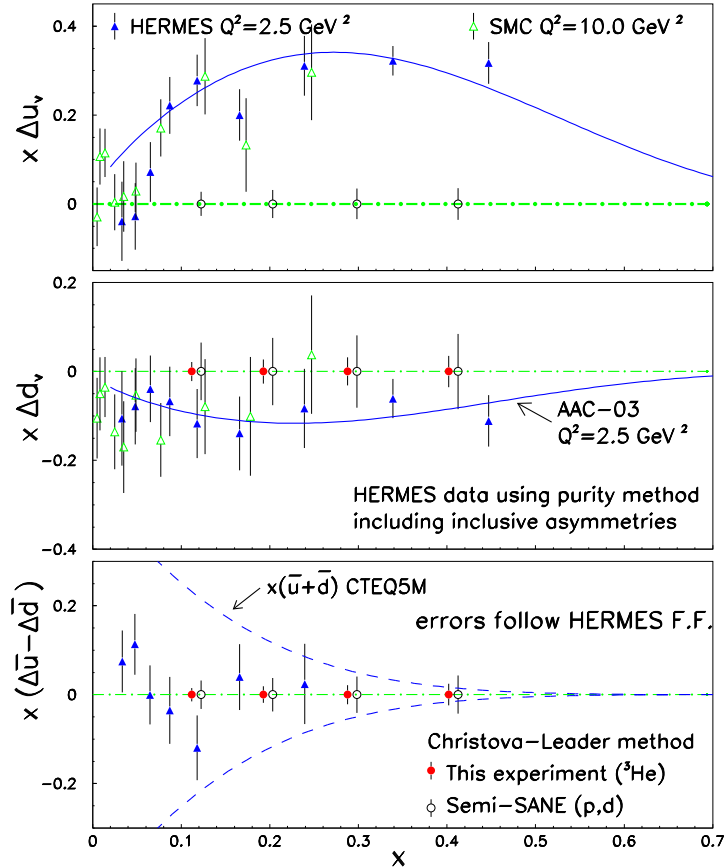


Figure 19: The expected statistical accuracy of $x\Delta d_v$ corresponding to the Christova-Leader method, following the fragmentation function ratios of HERMES. The expected uncertainties of semi-SANE Δu_v are used in constructing $x\Delta d_v$ and $x(\Delta \bar{u} - \Delta \bar{d})$. The published HERMES purity results^{2,3}, which included a combined data set of inclusive and semi-inclusive asymmetries, are also shown. Uncertainties following the KLC fragmentation function are shown in Fig. 30 in Appendix.

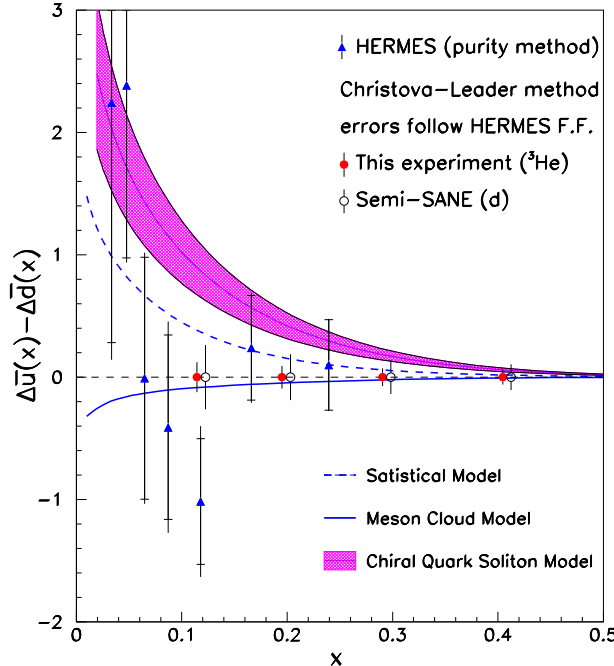


Figure 20: The expected statistical accuracy of $\Delta\bar{u} - \Delta\bar{d}$ corresponding to the leading order Christova-Leader method. Error propagation follows the HERMES fragmentation function ratio. The expected uncertainties of semi-SANE proton data are used in constructing $\Delta\bar{u} - \Delta\bar{d}$. The published HERMES purity results², which included a combined data set of inclusive and semi-inclusive asymmetries, are also shown. Model predictions are from the Statistical Model⁴², Meson Cloud Model¹⁷ and the Chiral Quark Soliton Model³⁹.

ratios make the outcome even more robust. With much more equations than unknowns, we can even allow this ratio to be a floating parameter in solving the linear equation system.

At the high- x bin ($x = 0.413$), this experiment overlaps with the recent Hall A experiment¹⁴ (E99-117) which extracted ratios of $(\Delta u + \Delta \bar{u})/(u + \bar{u})$ and $(\Delta d + \Delta \bar{d})/(d + \bar{d})$ from the inclusive asymmetry A_{1n} . The consistency check between semi-inclusive data from this experiment and the inclusive data of E99-117 provides the validity test of the various flavor decomposition methods.

Impact to NLO QCD global fit: sea and gluon polarization moments

Constraints to the moments of $\Delta\bar{u}$, $\Delta\bar{d}$ and Δs with the expected ${}^3\text{He}$ data in the next-to-leading order global fit¹² are shown in Fig. 21. The constraint on Δg moments coming from the addition of data of this experiment, as shown in Fig. 22 (left), is as stringent as the projected-2007 $A_{LL}^{\pi^0}$ data from PHENIX at RHIC, shown in Fig. 22 (right). The main reason of this sensitivity is because Δg is obtained in the global fit through the Q^2 -evolutions, but always coupled with the sea distribution. Once the sea distribution can be reasonably fixed with the semi-inclusive data, gluon

polarization is better constrained through the global fit. The impact to the moment of u and d -quark polarization is shown in Fig. 23.

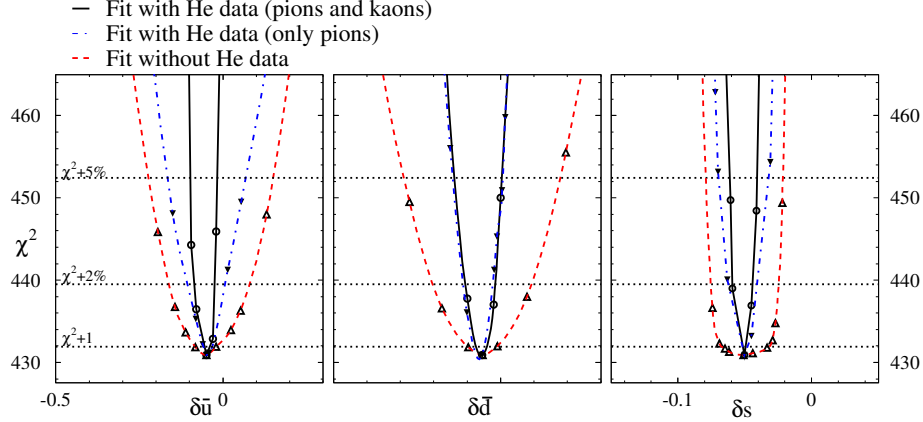


Figure 21: The constraints to the moments of sea polarization in NLO global fit by this experiment¹². The red dashed lines are the constraint by the existing data, the blue dot-dashed lines are the constraints by adding the pion data from this experiment, the solid lines are the constraints by adding both pion and kaon data of this experiment. The horizontal dotted lines are corresponding to an overall χ^2 change of $\chi^2 + 1$ ($\pm 1\sigma$ in pPDF), $\chi^2 + 2\%$ and $\chi^2 + 5\%$ in the global fit.

7 Relation with other experiments

- Hall C semi-SANE experiment. In many aspects, this experiment is very similar to the Hall C semi-SANE experiment (E04-113) which was approved by PAC-26 for polarized proton and deuteron runs. By expanding SIDIS measurements to a high density polarized ${}^3\text{He}$ target we will obtain much precise information on the neutron asymmetries and the d -quark polarization (a factor of three reduction in statistical uncertainties, see Appendix). This crucial improvement provide us with the first opportunity to definitely address the issue of flavor asymmetry in polarized sea.

The two experiments will run with almost identical kinematics such that similar cut can be applied in a combined analysis..

- Hall B polarized target data were originally collected for inclusive measurements in order to extract A_{1p} and A_{1d} . Part of data taken in year 2000 with 5.7 GeV beam (eg1b) has been analyzed for $(e, e'\pi)$ reactions. However, the physics goals addressed in this proposal can not be achieved in analyzing the existing eg1b data simply because the sensitivity to Δd is very limited.

At 6 GeV beam energy, to keep Q^2 and W as high as possible in order to access the deep-inelastic region, the direction of momentum transfer \vec{q} must be kept very close to the direction of the beam, to within 10° . Therefore,

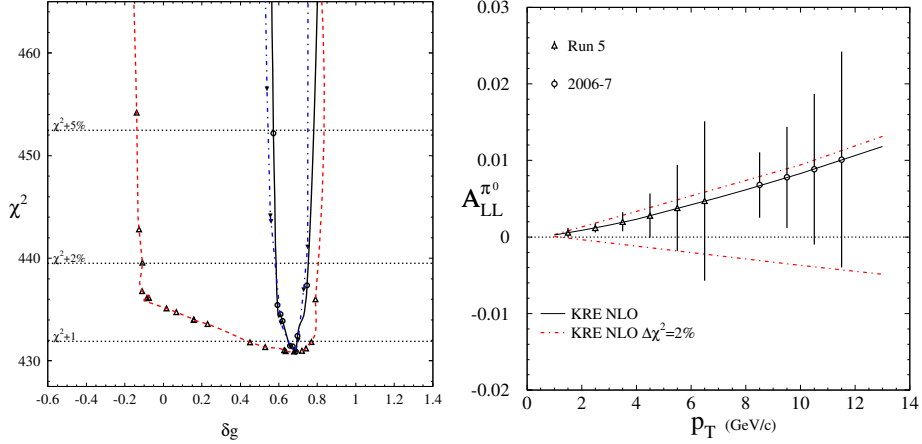


Figure 22: The constraint to the moment of the gluon polarizations in NLO global fit by this experiment (left) is compared with that from the expected RHIC-PHENIX $A_{LL}^{\pi^0}$ data (right). On the left side, red dashed line: existing data, blue dot-dashed line: adding only pion data of this experiment, solid line: adding both pion and kaon data of this experiment. On the right panel, the region covered between the two dot-dashed lines is corresponding to the $\chi^2 + 2\%$ crossover region with the red-dashed line on the left panel.

very forward-angle hadron detection is crucial in order to detect the leading hadrons in the fragmentation and to have a clear separation between the current fragmentation and the target fragmentation regime. In addition, a cut in W' as high as possible is desired in order to access the deep inelastic region and to avoid the exclusive channels and the resonance production channels. While Hall A septum+HRS can reach 6.0° , the nominal CLAS acceptance shrinks rapidly for hadrons coming out at angles less than 20° .

At hadron momentum larger than 1.5 GeV/c, the CLAS particle ID becomes problematic, especially for kaons. Kaon contamination in the A_{1N}^π asymmetry can not be avoided. In addition, since positively charged and negatively charged hadrons are bent into opposite directions, differences in the phase spaces and the detection efficiencies are expected, it is rather difficult to construct the combined $\pi^+ \pm \pi^-$ asymmetries from the existing eg1b data.

- HERMES has no plan to take more longitudinal polarized target data.
- The COMPASS experiment focus on low- x region, its kinematics ($x < 0.1$) does not overlap with this experiment.
- RHIC spin program, with the planned luminosity upgrade¹³, will measure Δq through weak W^\pm decays at $Q^2 = m_W^2$.
- JLab 12 GeV. Jefferson Lab is actively pursuing the opportunity of an energy upgrade to 12 GeV. Semi-inclusive experiments will be a rich physics program

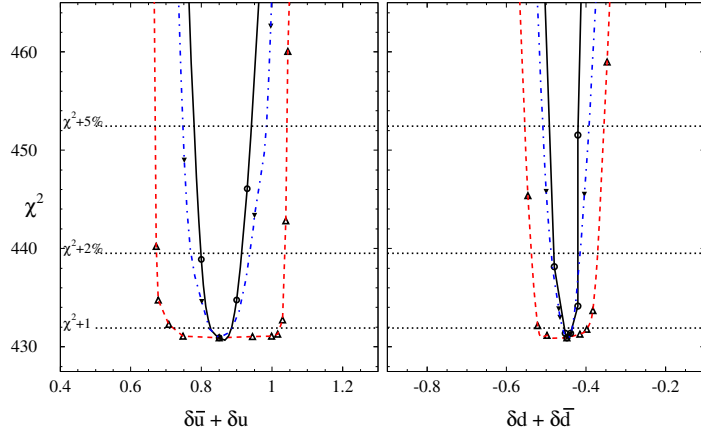


Figure 23: The constraints to the moments of u and d -quark polarization in NLO global fit by this experiment¹². The red dashed lines are the constraint by the existing data, the blue dot-dashed lines are the constraints by adding the pion data from this experiment, the solid lines are the constraints by adding both pion and kaon data of this experiment.

with the upgrade which will include spin-flavor decomposition and transverse spin physics.

8 Collaboration and responsibility

Members of this collaboration have run many Hall A polarized ${}^3\text{He}$ target experiments and have been heavily involved in other Hall A BigBite experiments (such as the G_{En} and the neutron transversity experiment). This proposal has been adopted as a Hall A Collaboration experiment after an extensive internal review. We expect JLab will handle installation of the septum magnet and the BigBite spectrometer if it is not already in place from an earlier operation.

9 Summary

We propose to measure the beam-target double-spin asymmetries in semi-inclusive deep-inelastic $\vec{n}(\vec{e}, e'\pi^+)X$ and $\vec{n}(\vec{e}, e'\pi^-)X$ reactions (kaons as by-products) on a longitudinally polarized ${}^3\text{He}$ target, in the kinematic region of $x = 0.12 \sim 0.41$ at $Q^2 = 1.21 \sim 3.14 \text{ GeV}^2$ with the leading hadron at $z \approx 0.5$. Since the neutron asymmetries are most sensitive to d -quark polarization, this experiment will dramatically improve our knowledge of Δd . The experiment will focus on the measurement of the combined asymmetry, $A_{1He}^{\pi^+ - \pi^-}$, in which the ratio of π^- to π^+ cross-sections will be well-determined. When changing from π^- to π^+ reaction the electron acceptance in BigBite and the pion acceptance in HRS will remain touched, and the pion detection efficiencies in HRS can be well-measured. Based on the measurement of $A_{1He}^{\pi^+ - \pi^-}$, and $A_{1p}^{\pi^+ - \pi^-}$ from Hall C semi-SANE, a leading-order as well as a next-to-leading order

spin-flavor decomposition of Δu_v and Δd_v can be made following the Christova-Leader method. The much improved sensitivity to $\Delta \bar{u} - \Delta \bar{d}$, compared with that of semi-SANE, will definitely provide us with the first opportunity to discover the possible polarized sea asymmetry. The high precision data from this experiment will also be used as inputs to a global next-to-leading order QCD analysis to put strong constraints on quark helicity distributions, and indirectly constrains gluon polarization to the level comparable to what RHIC-spin promised to deliver.

The recently constructed BigBite spectrometer, in the same detector configuration as in Hall A “ G_{En} ” and “neutron transversity” experiments, will be used to detect the scattered electrons at 30° . The left-HRS spectrometer, with its septum magnet at 6° , will be used to detect the leading hadrons in coincidence (at $p_h = 2.4$ GeV/c, $z \approx 0.5$). All experimental apparatus exist in Hall A and no special requirement is needed for the BigBite detectors beyond its standard configuration in the “ G_{En} ” experiment.

We believe that this experiment will have a strong impact to our understandings of nucleon spin structure, and put Jefferson Lab in strong competition with the RHIC-spin program. A total of 24 days of beam time is requested in Hall A.

A HERMES purity method and results

The HERMES analysis explicitly assumed the $x - z$ factorization of Eq. 1 at the leading order, the asymmetries are related to the parton polarizations through linear relations as:

$$A_{1N}^h(x, Q^2, z) = \frac{\sum_f e_f^2 \Delta q_f(x, Q^2) \cdot D_f^h(z, Q^2)}{\sum_f e_f^2 q_f(x, Q^2) \cdot D_f^h(z, Q^2)}. \quad (35)$$

The HERMES analysis used the “purity method” to achieve leading order flavor decomposition⁶⁴. In Eq. 35, a “purity matrix” $\mathcal{P}_f^h(x, Q^2, z)$ was defined such that:

$$A_{1N}^h(x, Q^2, z) \equiv \sum_f \mathcal{P}_f^h(x, Q^2, z) \cdot \frac{\Delta q_f(x, Q^2)}{q_f(x, Q^2)}, \quad (36)$$

where

$$\mathcal{P}_f^h(x) = \frac{e_f^2 q_f(x) \int dz D_f^h(z)}{\sum_i e_i^2 q_i(x) \int dz D_i^h(z)}, \quad (37)$$

and the explicit Q^2 notation has been omitted for simplicity. The “purity method” integrates over all the experimentally allowed z -range such that SIDIS events are included as much as possible to improve statistical accuracy. The exact values of $\mathcal{P}_f^h(x, Q^2, z)$ in the HERMES analysis were obtained through a detailed Monte Carlo simulation which was based on the Lund fragmentation model⁶⁵ and take into account the experimental phase space and detector efficiencies. The parameters used in the fragmentation model were fine-tuned in order to reproduce the measured hadron yields.

Integrating over hadrons with $0.2 < z < 0.8$, HERMES extracted five flavor quark polarizations:

$$\vec{Q} = (x\Delta u, x\Delta d, x\Delta \bar{u}, x\Delta \bar{d}, x\Delta s), \quad (38)$$

from a data base of measured double-spin asymmetries

$$\vec{A} = (A_{1p}^{\pi^+}, A_{1p}^{\pi^-}, A_{1d}^{\pi^+}, A_{1d}^{\pi^-}, A_{1d}^{K^+}, A_{1d}^{K^-}, A_{1p}, A_{1d}) \quad (39)$$

by solving the relations of $\vec{A} = \mathcal{P}_f^h(x) \cdot \vec{Q}$. The HERMES data on proton and deuteron asymmetries² are shown in Fig. 24 and 25 in comparison with the SMC data⁴. The ratio of $\Delta q/q$ for each flavor from the purity method is shown in Fig. 26

An independent effort of flavor decomposition using the leading order Christova-Leader method has also been carried out in the HERMES analysis³, although not presented in the published data. However, due to the unfavorable π^-/π^+ ratio at higher- x bins in HERMES, the statistical uncertainties of the Christova-Leader method are rather large compared to that of the purity method, as shown in Fig. 27

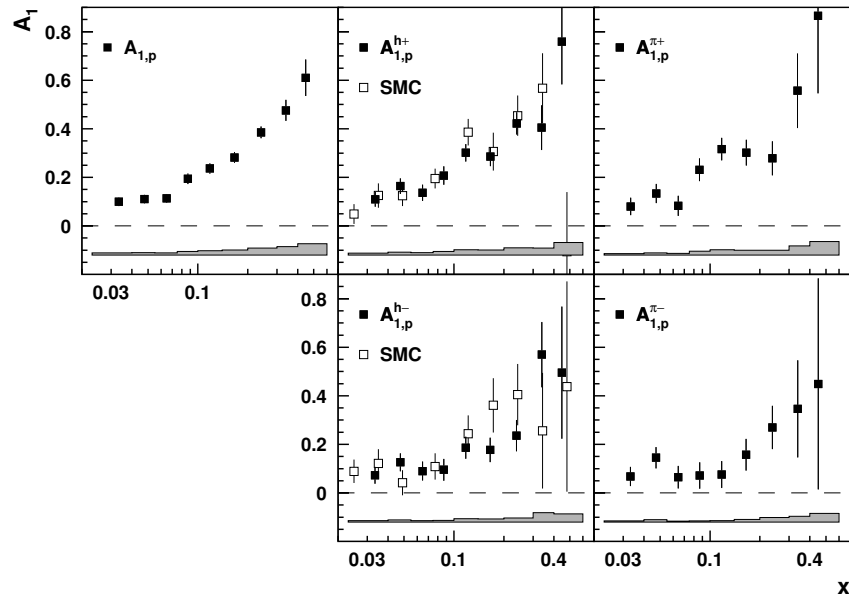


Figure 24: The double-spin asymmetries on proton A_{1p}^h form HERMES² and SMC⁴.

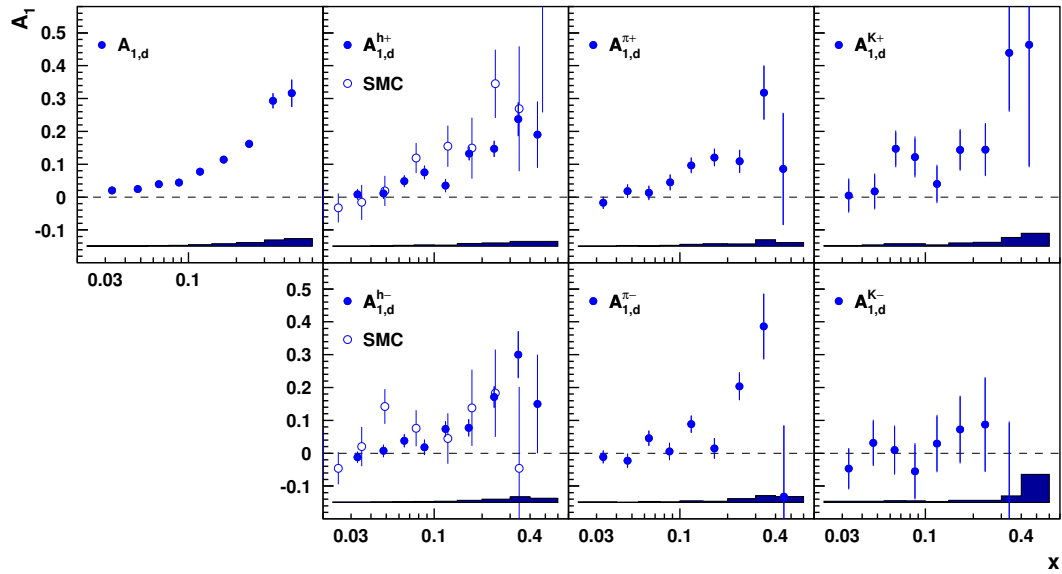


Figure 25: The double-spin asymmetries on deuteron A_{1d}^h form HERMES² and SMC⁴.

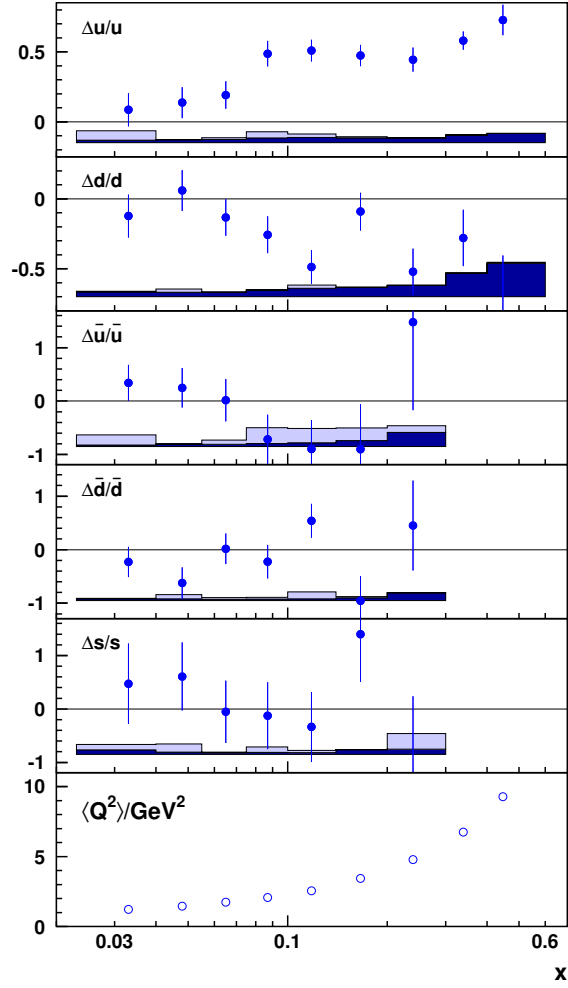


Figure 26: The HERMES results² of the polarized quark distributions $\Delta q(x)/q(x)$ at a common scale of $Q^2 = 2.5 \text{ GeV}^2$.

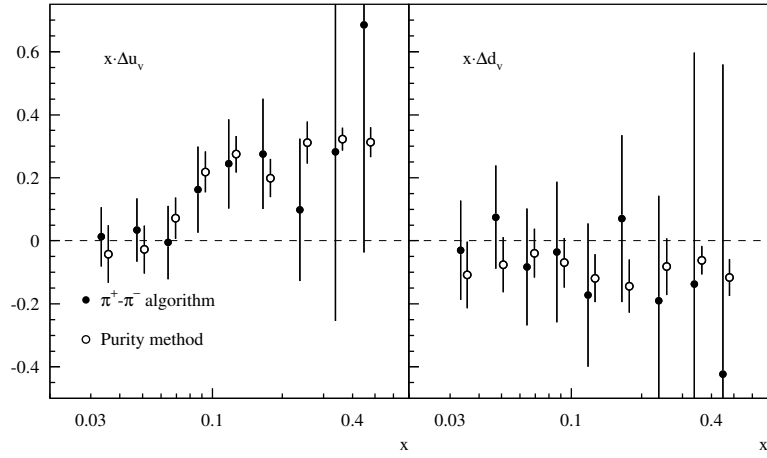


Figure 27: Statistical error comparison of the HERMES purity method (open circles) with the HERMES Christova-Leader method analysis³ (solid circles).

B Details of flavor decomposition

Following the short-hand notation of Ref⁹, we take the spin-independent cross section as:

$$\sigma^h(x, z) = \sum_f e_f^2 q_f(x) \cdot D_{q_f}^h(z), \quad (40)$$

and the spin-dependent cross section as:

$$\Delta\sigma^h(x, z) = \sigma_{++}^h - \sigma_{+-}^h = \sum_f e_f^2 \Delta q_f(x) \cdot D_{q_f}^h(z), \quad (41)$$

where σ_{ij}^h refers to an electron of helicity- i and nucleon of helicity- j . Assuming isospin symmetry and charge conjugation invariance, the number of quark to pion fragmentation functions is reduced to three types: the favored (D_π^+), the unfavored (D_π^-) and the s -quark (D_s^π) fragmentation functions:

$$\begin{aligned} D_\pi^+ &\equiv D_u^{\pi+} = D_d^{\pi-} = D_{\bar{u}}^{\pi-} = D_{\bar{d}}^{\pi+}, \\ D_\pi^- &\equiv D_u^{\pi-} = D_d^{\pi+} = D_{\bar{u}}^{\pi+} = D_{\bar{d}}^{\pi-}, \\ D_s^\pi &\equiv D_s^{\pi+} = D_{\bar{s}}^{\pi-} = D_{\bar{u}}^{\pi+} = D_{\bar{d}}^{\pi+}. \end{aligned} \quad (42)$$

For the quark to kaon fragmentation functions, the following relations are valid under charge conjugation[?]:

$$\begin{aligned} D_K^+ &\equiv D_u^{K+} = D_{\bar{u}}^{K-} = D_s^{K+} = D_{\bar{s}}^{K-}, \\ D_K^- &\equiv D_u^{K-} = D_{\bar{u}}^{K+} = D_s^{K-} = D_{\bar{s}}^{K+}, \\ D_d^K &\equiv D_d^{K+} = D_{\bar{d}}^{K+} = D_{\bar{d}}^{K-} = D_d^{K-}. \end{aligned} \quad (43)$$

For this experiment, which covers $0.12 < x < 0.43$, we will assume a symmetrical strange quark distribution and polarization ($s(x) = \bar{s}(x)$, $\Delta s(x) = \Delta \bar{s}(x)$) in the fixed- z purity method and neglect heavy quark contributions.

B.1 Spin-dependent and spin-independent cross sections

According to Eq. 40, semi-inclusive π^+ and π^- cross section on proton and neutron are:

$$\begin{aligned} 9\sigma_p^{\pi^+} &= (4u + \bar{d})D_\pi^+ + (4\bar{u} + d)D_\pi^- + (s + \bar{s})D_s^\pi, \\ 9\sigma_p^{\pi^-} &= (4u + \bar{d})D_\pi^- + (4\bar{u} + d)D_\pi^+ + (s + \bar{s})D_s^\pi, \\ 9\sigma_n^{\pi^+} &= (4d + \bar{u})D_\pi^+ + (4\bar{d} + u)D_\pi^- + (s + \bar{s})D_s^\pi, \\ 9\sigma_n^{\pi^-} &= (4d + \bar{u})D_\pi^- + (4\bar{d} + u)D_\pi^+ + (s + \bar{s})D_s^\pi, \end{aligned} \quad (44)$$

the explicit x, z, Q^2 dependence has been left out to save space whenever not causing confusion. The semi-inclusive K^+ and K^- cross sections are:

$$9\sigma_p^{K^+} = (4u + \bar{s})D_K^+ + (4\bar{u} + s)D_K^- + (d + \bar{d})D_d^K,$$

$$\begin{aligned}
9\sigma_p^{K^-} &= (4u + \bar{s})D_K^- + (4\bar{u} + s)D_K^+ + (d + \bar{d})D_d^K, \\
9\sigma_n^{K^+} &= (4d + \bar{s})D_K^+ + (4\bar{d} + s)D_K^- + (u + \bar{u})D_d^K, \\
9\sigma_n^{K^-} &= (4d + \bar{s})D_K^- + (4\bar{d} + s)D_K^+ + (u + \bar{u})D_d^K.
\end{aligned} \tag{45}$$

To get the spin-dependent cross sections ($\Delta\sigma^h$), one replaces the quark distribution in Eq. 44 and 45 with the quark polarization distribution.

B.2 The asymmetries expressed in “fixed-z purity”

The “fixed-z purity” is defined as the linear coefficients in front of Δq in the expression of double spin asymmetries, $A_1^h = \Delta\sigma^h/\sigma^h$. At the fixed value of z and x , these coefficients are obtained from the unpolarized parton distribution functions and the fragmentation function ratios. For example:

$$A_{1p}^{\pi^+} = \frac{4\Delta u + \Delta\bar{d} + (4\Delta\bar{u} + \Delta d)\lambda_\pi + 2\Delta s\xi_\pi}{4u + \bar{d} + (4\bar{u} + d)\lambda_\pi + 2s\xi_\pi}, \tag{46}$$

$$A_{1d}^{\pi^+} = \frac{4(\Delta u + \Delta d) + \Delta\bar{u} + \Delta\bar{d} + (\Delta u + \Delta d + 4(\Delta\bar{u} + \Delta\bar{d}))\lambda_\pi + 4\Delta s\xi_\pi}{4(u + d) + \bar{u} + \bar{d} + (u + d + 4(\bar{u} + \bar{d}))\lambda_\pi + 4s\xi_\pi}, \tag{47}$$

$$A_{1He}^{\pi^+} = \frac{8\Delta u + 4\Delta d + \Delta\bar{u} + 2\Delta\bar{d} + (\Delta u + 2\Delta d + 8\Delta\bar{u} + 4\Delta\bar{d})\lambda_\pi + 6\Delta s\xi_\pi}{8u + 4d + \bar{u} + 2\bar{d} + (u + 2d + 8\bar{u} + 4\bar{d})\lambda_\pi + 6s\xi_\pi}, \tag{48}$$

$$A_{1p}^{K^+} = \frac{4\Delta u + \Delta s + (4\Delta\bar{u} + \Delta d)\lambda_K + (\Delta d + \Delta\bar{d})\xi_K}{4u + s + (4\bar{u} + s)\lambda_K + (d + \bar{d})\xi_K}, \text{etc.} \tag{49}$$

where the fragmentation function ratios are defined as:

$$\begin{aligned}
\lambda_\pi(z) &= D_\pi^-(z)/D_\pi^+(z), & \xi_\pi(z) &= D_s^\pi(z)/D_\pi^+(z), \\
\lambda_K(z) &= D_K^-(z)/D_K^+(z), & \xi_K(z) &= D_d^K(z)/D_K^+(z).
\end{aligned} \tag{50}$$

C NLO global fit to DIS and SIDIS Data

The NLO global fit¹² to the existing DIS and SIDIS data are shown in Fig. 28.

D Comparison of statistical uncertainties with semi-SANE

The semi-SANE projected proton and deuteron measurements are translated into neutron asymmetries and plotted in Fig. 29.

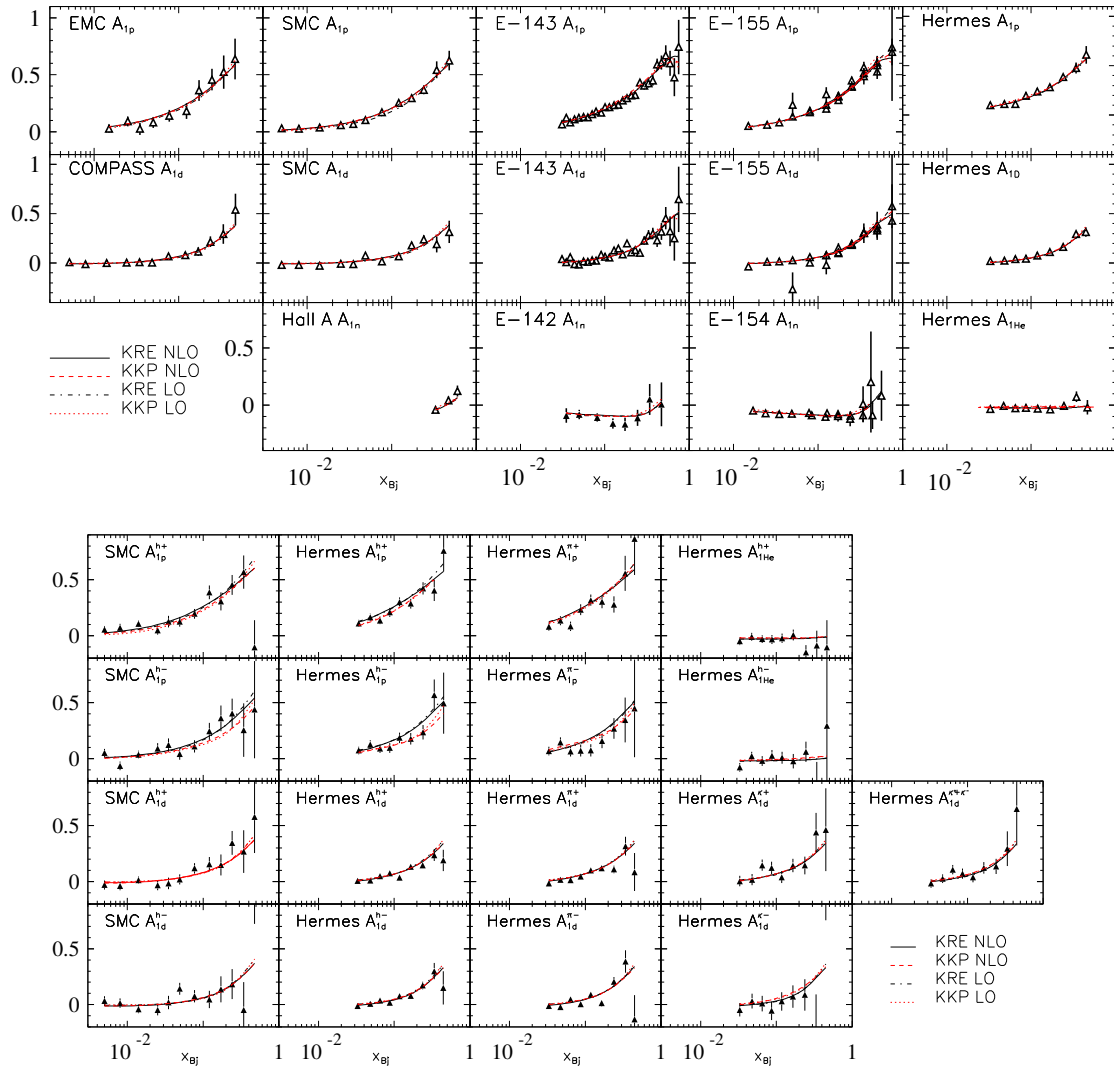


Figure 28: NLO global fit¹² to DIS data (top) and SIDIS data (bottom).

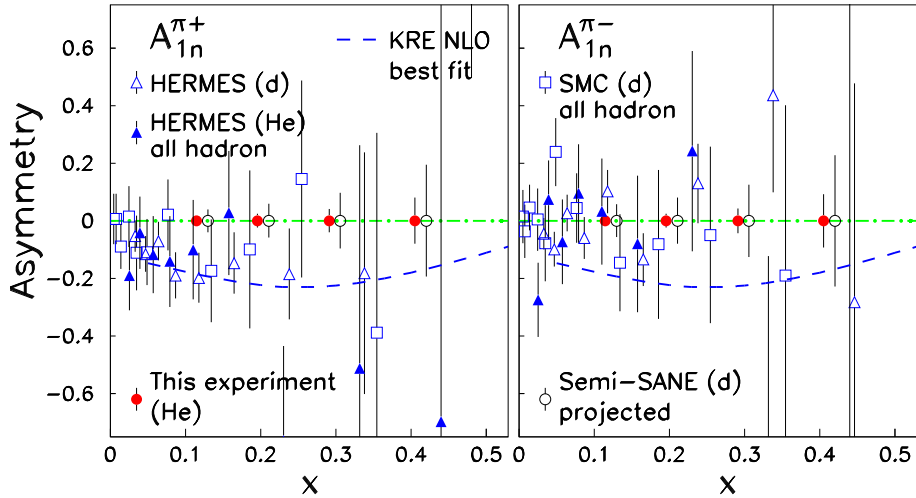


Figure 29: Same as in Fig. 18. The expected statistical accuracies of A_{1n}^π are compared with HERMES deuteron asymmetries² translated into neutron asymmetries, and the SMC deuteron asymmetries translated into neutron. The semi-SANE projected deuteron measurements are also translated into neutron asymmetries for easy comparison. This experiment will improve upon the semi-SANE statistical uncertainties by a factor of three.

References

1. L. L. Frankfurt, M. I. Strikman, L. Mankiewicz, A. Schafer, E. Rondio, A. Sandacz and V. Papavassiliou, *Phys. Lett. B* **230**, 141 (1989); F. E. Close and R. G. Milner, *Phys. Rev. D* **44**, 3691 (1991).
2. HERMES collaboration, *Phys. Rev. Lett.* **92**, 012005 (2004), and *Phys. Rev. D* **71**, 012003 (2005).
3. J. Wendland, Ph.D. Dissertation, Simon Fraser University, September (2003), and private communications, J. Wendland and A. Miller, June 2005.
4. The Spin Muon Collaboration, *Phys. Lett. B* **420**, 180 (1998).
5. H. Avakian, for the CLAS Collaboration, the proceeding of the “X-th Workshop on High Energy Spin Physics”, September 16-20, 2003.
6. R. Ent and P. Bosted, private communications.
7. Xiangdong Ji, Jian-Ping Ma and Feng Yuan, hep-ph/0404183.
8. Xiangdong Ji, Jian-Ping Ma and Feng Yuan, hep-ph/0405085.
9. E. Christova and E. Leader *Phys. Lett. B* **468**, 299 (1999) and *Nucl. Phys. B* **607**, 369 (2001).
10. JLab experiment E04-113, X. Jiang, P. Bosted, D. Day and M. Jones co-spokespersons.
11. D. de Florian and R. Sassot, *Phys. Rev. D* **62**, 094025 (2000), and D. de Florian, O. A. Sampayo and R. Sassot, *Phys. Rev. D* **57**, 5803 (1998)
12. D. de Florian, G. A. Navarro and R. Sassot, *Phys. Rev. D* **71**, 094018 (2005), and private communications (2005).

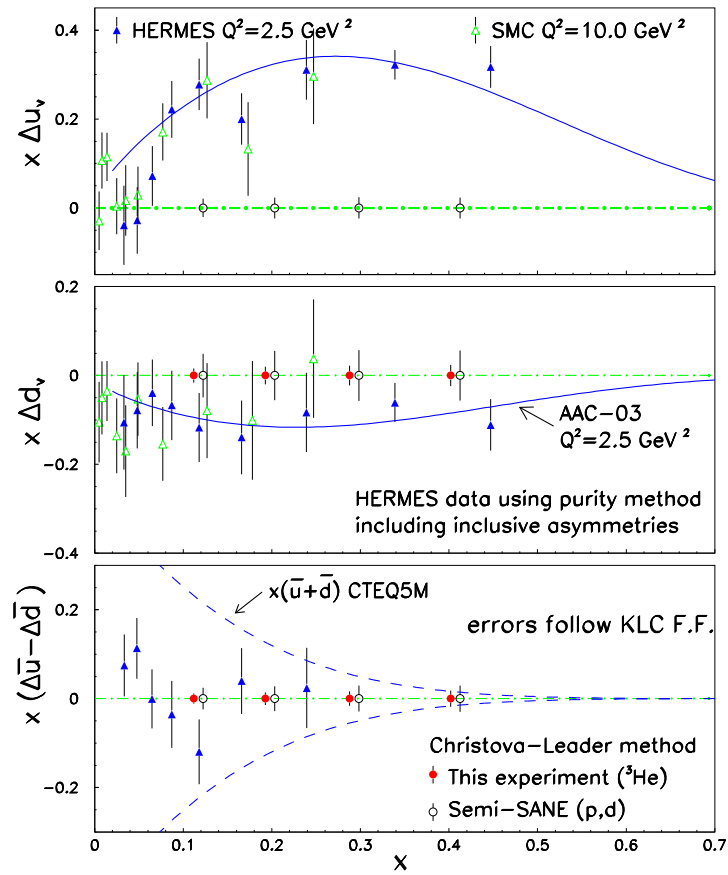


Figure 30: Same as in Fig. 19, except following the fragmentation function ratios of KLC. The expected statistical accuracy of $x\Delta d_v$ corresponding to the Christova-Leader method.

13. G. Bunce, N. Saito, J. Soffer and W. Vogelsang, Ann. Rev. Nucl. Part. Sci. **50**, 525 (2000).
14. Jefferson Lab Hall A, X. Zheng, *et al.*, *Phys. Rev. Lett.* **92**, 012004 (2004).
15. Jefferson Lab Hall A, K. Kramer *et al.*, nucl-ex/0506005.
16. Dressler, B. *et al.*, *Eur. Phys. J. C* **14**, 147 (2000).
17. F. G. Cao, A. I. Signal, *Eur. Phys. J. C* **21**, 105 (2001).
18. Glück, M. *et al.*, *Phys. Rev. D* **63**, 094005 (2001).
19. Blümlein, J., Böttcher, H., hep-ph/0203155, *Nucl. Phys. B*, (2002) in press.
20. HERMES collaboration, K. Ackerstaff *et al.*, *Phys. Lett. B* **464**, 123 (1999).
21. D. Graudenz, *Nucl. Phys. B* **432**, 351 (1994).
22. D. de Florian, C. A. Garcia Canal, R. Sassot, *Nucl. Phys. B* **470**, 195 (1996).
23. Marco Stratmann and Werner Vogelsang, *Phys. Rev. D* **64**, 114007 (2001)
24. S. Kretzer, *Phys. Rev. D* **62**, 054001 (2000).
25. B. A. Kniehl, G. Kramer, and B. Potter, *Nucl. Phys. B* **582**, 514 (2000).
26. A. N. Sissakian, O. Yu. Shevchenko and O. N. Ivanov, *Phys. Rev. D* **70**, 074032 (2004)
27. A. N. Sissakian, O. Yu. Shevchenko and O. N. Ivanov, hep-ph/0505012.
28. E. A. Hawker, *et al.*, *Phys. Rev. Lett.* **80**, 3715 (1998).
29. J. C. Peng, *et al.*, *Phys. Rev. D* **58**, 092004 (1998). *Eur. Phys. J. C* **5**, 461 (1998).
30. J.-C. Peng, *Eur. Phys. J. A* **18**, 395 (2003).
31. E. Eichten, I. Hinchliffe, C. Quigg, *Phys. Rev. D* **45**, 2269 (1992).
32. A. W. Thomas, *Phys. Lett. B* **126**, 97 (1983).
33. R. J. Fries, A. Schafer, *Phys. Lett. B* **443**, 40 (1998).
34. K. G. Boreskov, A. B. Kaidalov, *Eur. Phys. J. C* **10**, 143 (1999).
35. S. Kumano, M. Miyama, *Phys. Rev. D* **65**, 034012 (2002).
36. R. J. Fries, A. Schafer, C. Weiss, hep-ph/0204060.
37. M. Gluck *et al.*, *Phys. Rev. D* **63**, 094005 (2001).
38. F. M. Steffens, *Phys. Lett. B* **541**, 346 (2002).
39. B. Dressler *et al.*, hep-ph/9809487.
40. M. Wakamatsu, T. Watabe, *Phys. Rev. D* **62**, 017506 (2000).
41. A. Dorokhov, hep-ph/0112332.
42. C. Bourrely, J. Soffer and F. Buccella, *Eur. Phys. J. C* **23**, 487 (2002), hep-ph/0502180 and private communications, June,(2005).
43. R. S. Bhalerao, *Phys. Rev. C* **63**, 025208 (2001).
44. A. Efremov, *et al.*, *Nucl. Phys. A* **711**, 84 (2002), and A. Efremov, *et al.*, *Phys. Rev. D* **67**, 114014 (2003).
45. HERMES collaboration, A. Airapetian *et al.*, *Phys. Rev. Lett.* **94**, 012002 (2005).
46. Jefferson Lab experiment E03-004, X. Jiang, J.-P. Chen and J.-C. Peng co-spokespersons.
47. Frank E. Close and Nathan Isgur, *Phys. Lett. B* **509**, 81 (2001)
48. C. J. Bebek, *et al.*, *Phys. Rev. Lett.* **30**, 624 (1973).

49. G. Drews, *et al.*, *Phys. Rev. Lett.* **41**, 1433 (1978).
50. G. Cates, K. McCormick, B. Reitz and B. Wojtsekhowski, Jefferson Lab experiment E02-013: “Measurement of the Neutron Electric Form Factor G_E^n at High Q^2 ” (2002).
51. P. J. Mulders, hep-ph/0010199, “Current fragmentation in semi-inclusive lepton production”.
52. T. Sloan, G. Smadja and R. Voss, *Phys Rep.* 162 (1988) 45.
53. P. Deltiarenko, private communications, 2005.
54. Lai, H.L. *et al.*, *Eur. Phys. J.* **C12**, 375 (2000).
55. S. Kretzer, E. Leader and E. Christova, *Eur. Phys. J. C* **22**, 269 (2001).
56. D. Gaskell, private communication.
57. P. Geiger, Ph.D. Dissertation, Ruprecht-Karls-University, Heidelberg (1998).
58. JLab experiment E03-109, “Spin Asymmetries on the Nucleon Experiment” (SANE), S. Choi, Z.-E. Meziani and O.A. Rondon co-spokespersons.
59. A. Nogga, Ph. D. thesis, Ruhr-Universität Bochum, Bochum, Germany (2001), p.72.
60. J.L. Friar *et al.*, *Phys. Rev. C* **42**, 2310 (1990).
61. C. Ciofi degli Atti *et al.*, *Phys. Rev. C* **48**, R968 (1993).
62. F. Bissey *et al.*, *Phys. Rev. C* **64**, 024004 (2001);
63. M. Sargsian, private communications, (2004).
64. J.M. Niczyporuk and E.E.W. Bruins, *Phys. Rev. D* **58**, 091501 (1998).
65. B. Anderson, G. Gustafson, G. Ingemann, and T. Sjöstrand, *Phys. Rep.* **97**, 31 (1983).